Theses and Dissertations   Student Graduate Works

3-2004

Atmospheric Simulation Using a Liquid Crystal Wavefront Controlling Device

Matthew R. Brooks

ATMOSPHERIC SIMULATION USING A LIQUID CRYSTAL WAVEFRONT

CONTROLLING DEVICE

THESIS

Matthew R. Brooks, 2nd Lieutenant, USAF

AFIT/GE/ENG/04-01

DEPARTMENT OF THE AIR FORCE

AIR UNIVERSITY

AIR FORCE INSTITUTE OF TECHNOLOGY

Wright Patterson Air Force Base, Ohio

AFIT/GE/ENG/04-01

ATMOSPHERIC SIMULATION USING A LIQUID CRYSTAL WAVEFRONT

CONTROLLING DEVICE

THESIS

Presented to the Faculty

Department of Electrical and Computer Engineering

Graduate School of Engineering and Management

Air Force Institute of Technology

Air University

Air Education and Training Command

in Partial Fulfillment of the Requirements for the

Degree of Master of Science in Electrical Engineering

Matthew R. Brooks, BS

2nd Lieutenant, USAF

23 March 2004

AFIT/GE/ENG/04-01

ATMOSPHERIC SIMULATION USING A LIQUID CRYSTAL WAVEFRONT
CONTROLLING DEVICE

Matthew R. Brooks, BS
2nd Lieutenant, USAF

Approved:

_____/signed/_____	_2/27/04_
Matthew E. Goda, Ph.D.	Date
Thesis Advisor	
_____/signed/_____	_2/24/04_
Won B. Roh, Ph.D.	Date
Committee Member	
_____/signed/_____	_2/24/04_
Steven C. Gustafson, Ph.D.	Date
Committee Member	

Acknowledgements

Effort that has led to the completion of this thesis rested upon my shoulders, but was lightened by many. I would first like to thank my thesis advisor, Major Matthew Goda, Ph.D., for his guidance, knowledge, and unending ability to spend time assisting me even when his own plate was very full. I also appreciate the enthusiasm and suggestions of those in my sponsoring organization (AFRL/SNJT), especially that of Jack Parker, Ph.D. Your expressed interest and check-ups helped inspire and remind me of the importance of my work. I am greatful also to Matthew Whitely, Ph.D., and Eric Magee, Ph.D., for their help using Wavetrain and allowing me to get familiar with SLM's early in the game. To my classmates of GE-04M, thank you for helping me keep a light heart through the late nights. I owe much to my parents for giving me a foundation that has enabled me to get to where I am today. Let my achievements be a reflection of your love. And finally, I want to acknowledge the one who supported me most, my wife. Thank you for always being there in everything I do. Staying up with me during countless late nights and dealing with my physical and mental absence must have been a challenge. I will never forget your unfaltering support. Finally I praise God on whom I depend. "I can do everything through Him who gives me strength." -Philippians 4:13

Matthew R. Brooks

<div align="center">

Table of Contents

</div>

List of Figures

ix

List of Tables

AFIT/GE/ENG/04-01

Abstract

Test and evaluation of laser warning devices is important due to the increased use of laser devices in aerial applications. In this thesis, an atmospheric aberrating system is developed to enable in-lab testing of laser warning devices. This system employs laser light at 632.8 nm from a Helium-Neon source and a spatial light modulator (SLM) to cause phase changes using a birefringent liquid crystal material.

Before the system can be used, the SLM phase response must be quantified to ensure proper manipulation of index of refraction. Additionally, diffraction from the SLM and real-world system scaling are addressed. Once completed, the atmospheric simulator is demonstrated and verified.

Control of the SLM is achieved by loading 256 level bitmaps which dictate the desired index of refraction changes (called phase screens). Phase screens are created using a Fourier series technique applied to an atmospheric model in the form of a power spectrum. Five laser propagation scenarios are created, each with a set of screens describing turbulence for a particular case. Outgoing radiation from the SLM is then measured using a CCD targetboard for intensity and a Shack-Hartmann wavefront sensor for phase. Comparing system output phase statistics to atmospheric theory reveals a moderate correlation in all turbulence cases indicating desired performance. Intensity statistics are compared to the log normal distribution governed by the weak fluctuation regime. An error analysis reveals that strong turbulence data matches theory but that weak turbulence data is inconclusive due to measurement precision issues. As an additional check on performance, a wave optics computer simulation is created analogous to the lab-bench design. Phase and intensity data affirm lab-bench results so that the aberrating SLM system can be operated confidently.

ATMOSPHERIC SIMULATION USING A LIQUID CRYSTAL WAVEFRONT CONTROLLING DEVICE

I. Introduction

1.1 Research Motivation

Laser devices have long been used in and around the battle field in a variety of systems. These systems include tracking, guidance, communication, sensing, and direct offense. As laser technology and beam control systems improve to become higher power and more diverse, the Air Force predicts laser weapons and systems to be increased threats. Laser weapons are a particular threat to pilots because of the critical need for pilot vision and the ease of causing damage to the human eye with moderate-power laser systems. There exists, however, a shortcoming in ability to detect the use of laser weapons because of their brief active times (through the full range of tens of seconds to femtoseconds) and frequent use in infrared spectral bands.

Several focused research efforts have developed sensors to detect and identify laser systems. These systems include laser devices used in missile guidance and communication. The similarity in these systems is that they are operated in aerial environments, where laser beams are directed in and through the Earth's atmosphere. As a result, laser energy is distorted and changed by index of refraction variations dictated by atmospheric turbulence. The consequence for laser beams is severe enough to be a significant factor in sensor effectiveness. Only a limited number of methods exist to test and evaluate these sensors. Thin, reflective membranes have been vibrated to create atmospheric-like aberrations, but do not readily match phase characteristics enough for critical system evaluation. Phase wheels have been used to create turbulence in the lab for longer periods, assuming "frozen flow." The drawback is that phase wheels prohibit dynamic variation of turbulence characteristics. Once the phase wheel is designed and manufactured, it cannot be changed. As of yet, no repeatable, flexible, and calibrated methods are available to simulate atmospheric aberrations in an enclosed laboratory environment. With the advent

1

of high-resolution controllable optic devices, it is possible to produce accurate atmospheric-like aberrating systems for laser beams. Such systems would allow test and evaluation of laser sensing devices in controlled environments to reduce the need for extensive field testing. Other possibilities include dynamic atmospheric simulators for any laser system evaluation and surrogate optic elements capable of replacing expensive or complex elements in a system.

1.2 Problem Statement

This research focuses on developing a rudimentary lab-bench tool that produces atmospheric-like aberrations in a optical system using a high resolution controllable optic device for test and evaluation of laser sensing devices.

1.3 Research Objectives

1. Demonstrate that atmospheric-like aberrations can be introduced in an optical system using a Spatial Light Modulator (SLM).

2. Characterize SLM behavior with attention to diffraction efficiency and non-linear behavior.

3. Verify valid system operation by comparing measured phase and intensity statistics to validated models.

1.4 Methodology

In the atmosphere, laser device effectiveness degrades due to beam spread and distortion caused by propagation through nonuniform media. In particular, the wavefront of the E-field describing light is manipulated by variations in refractive index of the media. A system that can mimic refractive index variations in the atmosphere can produce the same distortion effects on laser light that the real-world atmosphere would produce. A spatial light modulator (SLM) is used to implement this concept. The SLM consists of an array of pixels, where each pixel has a controllable index of refraction. Changing these individual pixel indices allows the wavefront passing through the device to be altered as

specified by the user. Therefore, it is possible to generate atmospheric phase screens (representations of how the atmosphere changes wavefronts) to imprint on the SLM and aberrate wavefronts as the atmosphere would do.

To produce phase screens, the atmosphere is modelled using established theory and data on refractive index variations. Random statistics of these variations can be captured using the structure function, which describes the randomness of the atmosphere. Using the structure function, the power spectrum describing the frequency content of index variations can be found [1]. Finally, the power spectrum leads to the desired phase screens through the use of a Fourier series technique. The structure function, power spectral density, and phase screen generation topics are defined and discussed in Chapter II. Resultant phase screens can then be translated to the SLM so that the phase of the wavefront is manipulated just as the atmosphere would shape the wavefront. In this way, atmospheric effects on optical systems can be reproduced in the lab. This thesis consists of a lab experiment and computer simulation of the system.

Experimentation. An optical test is performed in the lab to show that an SLM is a viable substitute for the real-world atmosphere in testing laser sensors. When implemented, the aberrating system consists of a laser source emitting light onto an SLM that reflects light toward the laser warning device being tested. To demonstrate this system, the laser warning device is replaced by two sensors to measure the SLM modification to the laser light. A helium-neon laser with $3\,\text{mW}$ output power is used for the source. Passing the HeNe beam through a spatial filter approximates a point source which is collimated using a doublet lens. Collimating the beam allows benchmark testing and facilitates system verification. To ascertain the effects of the SLM system, a targetboard CCD array and Shack-Hartmann wavefront sensor are used. The wavefront sensor measures the phase of the outgoing wavefront using an array of small lenses. To ensure that an accurate phase is measured, the wavefront must have a near uniform intensity before entering the aberrating system. Figure 1 shows an optical diagram of the experimental setup.

To control the aberrating system, a computer interface is used that requires 0 - 255 gray level images to communicate the phase modulation to the SLM. Phase screens
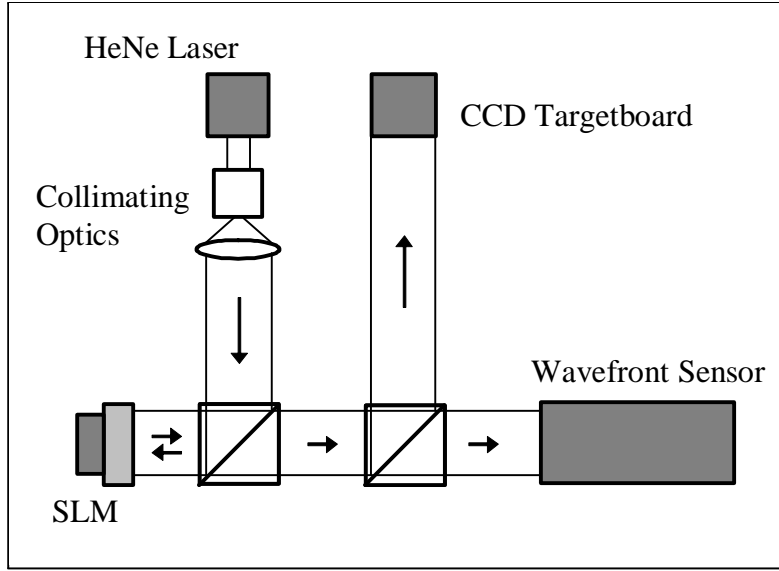
Figure 1   Optical setup of experiment with cameras and wavefront sensor

mimicking the atmosphere can be loaded to the SLM in the gray level format. In order to transcribe generated phase screens to the SLM so that light behaves in the desired manner, the phase screen pixel values must be modified based on the characteristics of the SLM. These characteristics include diffraction due to the geometry of the system and a non-linear phase delay behavior, both of which influence the wavefront in negative ways.

Simulation. Alongside the lab experiment that simulates atmospheric aberrations using the SLM, a computer simulation based on optical propagation and statistical theory verifies system behavior. Wavetrain, a software package for simulating optical systems by MZA Associates Corporation, is used to show this behavior. Wavetrain uses a series of light propagation algorithms based on the Fresnel integral discussed in Chapter II. Wavetrain also applies amplitude and phase screens at key locations in the simulation to represent apertures, turbulence, etc. Whenever a given field is input to a simulation, accuracy of simulation results greatly depends on the sample spacing and wavefront extent (amount of calculated wavefront). A field that is insufficiently sampled to represent the highest frequency components in both amplitude and phase produces erroneous results. Wavetrain allows the user to specify sample rates and grid sizes for input fields, propagation paths,

and fields incident on sensors (outputs). In addition, all these attributes can be user specified depending on the expected behavior at any of these locations in the system.

Wavetrain simulations are used for several purposes in this research. First, they help explore methods of countering undesirable characteristics of the SLM, such as diffraction effects. Second, simulations predict and verify overall system performance. This knowledge also helps explain unexpected system behavior by allowing easy variation of only one system attribute at a time.

1.5 Implications

This research demonstrates the ability of an SLM to introduce specified aberrations into an optical system for laser light. With the ability of the user to control exactly the aberrations present in the system, it is possible to evaluate system performance under usual and unusual conditions of use. The SLM device is of most use when testing optical systems operating in the Earth's atmosphere. Using atmospheric models in conjunction with phase screen generation to simulate atmospheric aberrations means completing lab tests where field testing was once required. A tool that accepts input from any known atmospheric model or data will enable a wide range of atmospheric behavior as well. Optical designs can be evaluated in-lab with simulated atmospheric conditions so that design improvements can be more quickly implemented. Air Force research involving laser warning systems will benefit from a tool that simulates atmospheric conditions in a lab environment. Specifically, design and evaluation times should be significantly reduced.

1.6 Summary

Evaluating optical systems for laser warning devices can be a cumbersome task in the development process because of the time needed for the complexities and logistics of field testing. Recreating real world optical conditions in the lab using a liquid crystal spatial light modulator allows realistic and controllable atmospheric aberrations to be inserted into an optical system so that testing time is shortened. Producing atmospheric aberrations is done by modeling the atmosphere and generating phase screens for use with an SLM. These phase screens are produced by a Fourier series implementation of the power

spectrum describing index of refraction variations. The SLM is then characterized so that abnormalities altering phase screen behavior can be compensated. These abnormalities include a nonlinear phase relationship to gray levels and diffraction due to a fill factor of 83% causing light to be diffracted in multiple directions off the optic axis. Correcting these issues allows for a controllable device that simulates many atmospheric conditions.

II. Theory

2.1 Introduction

Light propagation and atmospheric turbulence are the main topics of the research reported here. Origins of this theory are based on well-founded ideas with roots that go back several centuries when light and its behavior were first being explored. From that time, subsequent theories have been added to produce a better understanding of how light is manipulated in nature and how it can be controlled. The goal is to manipulate light in the same way that an atmosphere with given characteristics would manipulate it. Several indicators, such as amplitude and phase, are used to verify that light is manipulated as desired. To comprehend how this light manipulation is actualized, attention must be given to the areas of light diffraction, atmospheric turbulence, phase screen generation, phase modulation, wavefront sensing, and simulation.

2.2 Diffraction Theory

In testing laser warning systems, laser light travels from a source to a sensor. Laser light can be considered coherent. In the simplest case, a group of monochromatic light waves traveling together in a vacuum undergoes intensity and phase changes as it propagates. This behavior is known as diffraction and is essential to understand in designing an atmospheric aberrating system or modeling atmospheric effects on laser beams. Historically, light was thought to always move in straight lines unless reflected (by a reflective object) or refracted (by an interface between two media of unequal density). This was found to be only partially true in 1665 by a physicist named Francesco Grimaldi. He observed that light from a source coming through an aperture illuminated a spot on a screen at some distance who's diameter was larger than what the geometric theory of light predicted. Later in 1678, Christian Huygens theorized that a wavefront of light excites secondary sources that create their own wavefronts. The primary wave's position at a later time can be found by combining the secondary wavefronts. Still later, Thomas Young explained that coherent light can interfere with itself so that two light patches can be added to create a dark spot [2]. Combining these propagation and interference theories with

some assumptions about the shape of the wavefront leads to the Huygens-Fresnel equation

$$U(x,y) = \frac{e^{jkz}}{j\lambda z}e^{j\frac{k}{2z}(x^2+y^2)}\iint_{-\infty}^{\infty}\left\{U(\xi,\eta)e^{j\frac{k}{2z}(\xi^2+\eta^2)}\right\}e^{-j\frac{2\pi}{\lambda z}(x\xi+y\eta)}d\xi d\eta, \qquad (1)$$

where $U(\xi,\eta)$ is the initial complex wave and (x,y) are the transverse coordinates of the wave propagated a distance z. The Fresnel integral can be simplified by noticing that the resultant wavefront is found by multiplying the initial wavefront by a quadratic phase factor and then taking the Fourier transform. This Fourier transform quality benefits computation processes for simulation and verification in that calculating the resultant waveform uses a fast Fourier transform routine instead of implementing a double sum over all points in the output plane. The number of calculations required using the FFT is orders of magnitude less than that for evaluating the integral with sums. For long propagation distances, defined by the region in which $z \gg \frac{k(\xi^2+\eta^2)}{2}$, Equation 1 simplifies to a straight Fourier transform of the primary field [2]. Starting from Equation 1 and substituting $z \gg \frac{k(\xi^2+\eta^2)}{2}$ inside the quadratic phase factor to eliminate it gives

$$U(x,y) = \frac{e^{jkz}}{j\lambda z}e^{j\frac{k}{2z}(x^2+y^2)}\iint_{-\infty}^{\infty}\left\{U(\xi,\eta)\right\}e^{-j\frac{2\pi}{\lambda z}(x\xi+y\eta)}d\xi d\eta. \qquad (2)$$

Then, by definition of the Fourier transform, this equation becomes

$$U(x,y) = \frac{e^{jkz}}{j\lambda z}e^{j\frac{k}{2z}(x^2+y^2)}\mathcal{F}\{U(\xi,\eta)\}. \qquad (3)$$

Therefore, the behavior of light can be predicted at a certain propagation distance z. This knowledge of light propagation is the basis for the simulation tool that is used to verify the optical system in this research. It is also useful knowledge in theory development for light propagation through a turbulent atmosphere. Since this is the main focus of the research, the atmosphere will now be discussed in reference to how it can be modeled and its effects on light.

2.3 Atmospheric Turbulence Theory

The theory discussed above is only truly accurate for light propagation through a uniform medium with constant index of refraction. Light behaves quite differently when variations in index of refraction are present. The change in index of refraction first alters the speed of light, leading to a change in the shape of the wavefront of light. Understanding these changes and specifically what these changes look like in a random media like the atmosphere is important to producing an atmospheric model in phase screen form that will be used on the spatial light modulator. Along with the atmospheric model, there are several metrics of interest that are defined and used to measure system performance.

Atmospheric Modeling.   As briefly mentioned in Chapter I, the atmosphere can be described as a conglomeration of eddies that interact and exchange energy to form and divide into smaller eddies. It is necessary to define a region of eddy sizes that are of interest to the atmospheric model. The name for this region is the inertial subrange and is bounded by an inner scale l_o and outer scale L_o that denote the smallest and largest eddy sizes, respectively. For the model, each eddy is considered to have a relatively uniform temperature and pressure that directly affects the index of refraction experienced by light traveling through the eddy. When dealing with light propagation through the atmosphere, the index of refraction can be considered independent of time because of the short period that light occupies the eddy relative to the eddy's rate of change in position, size, etc. The index of refraction can be represented by

$$n(\mathbf{R}) = 1 + n_1(\mathbf{R}),\tag{4}$$

where $\mathbf{R}$ is a vector identifying a point of interest in space, 1 is the mean value of the index of refraction, and $n_1(\mathbf{R})$ is the deviation of the index from its mean value of one [1:56]. Using Equation 4, it is possible to arrive at the structure function to describe the variation of index of refraction in the atmosphere.

The structure function is necessary because it is not possible to exactly describe the index of refraction random process for all positions in space. There are too many random behaviors and variables to account for in a closed form solution. The index can only be

9

described in reference to stationary random functions. Over long spatial periods, the index of refraction is not a stationary random process, but over short spatial periods of interest to applications of laser propagation, the index is considered to have stationary increments [1:27]. In other words, it is possible to treat the index random process as stationary with emphasis on the function $n(\mathbf{R} + \mathbf{R}_1) - n(\mathbf{R}_1)$. Intuitively, the structure function of the index of refraction is the mean squared difference between the index of refraction at one point in space and the index at a point with some separation distance from the first point. The structure function of a random process $n(\mathbf{R})$ is defined by

$$D_n(\mathbf{R}_1, \mathbf{R}_2) = \langle [n(\mathbf{R}_1) - n(\mathbf{R}_2)]^2 \rangle, \tag{5}$$

where $\mathbf{R}_1$ and $\mathbf{R}_2$ are vectors describing points in space and $\langle \cdot \rangle$ denotes the ensemble average. In dealing with the index of refraction, it can be assumed that the random field describing the index is homogenous; the mean is independent of spatial position and the covariance is only dependent on the position difference of the points of interest $\mathbf{R}_2 - \mathbf{R}_1$. It can also be assumed that the index field is isotropic, meaning the covariance only depends on the separation distance of the points of interest ($|\mathbf{R}_2 - \mathbf{R}_1| = R$), and not their relative position [1:50]. A. N. Kolmogorov started with the definition of the structure function involving wind velocity (similar in form to Equation 5) and used dimensional analysis to show a $\frac{2}{3}$ power law behavior with respect to separation distance (R). This same method is applicable to the index of refraction and leads to the first part of Equation 6

$$D_n(R) = \begin{cases} C_n^2 R^{2/3} & , \quad l_o \ll R \ll L_o \\ C_n^2 l_o^{-4/3} R^2 & , \quad R \ll l_o \end{cases}, \tag{6}$$

where l_o and L_o are the inner and outer scales respectively. At small scale sizes below l_o, the structure function follows a squared relationship (second part of Equation 6) which is found by performing a Taylor Series expansion on the structure function for small separation distances [1:46]. C_n^2 is known as the structure constant and measures the strength variation in refractive index. It is defined so that Equation 6 has a coefficient of one. The

structure function is dependent on the separation distance R and has units of radians

$$D_n(R) = 6.88 \left(\frac{R}{r_o} \right)^{5/3} , \tag{7}$$

where r_o relates to turbulence strength and is defined and discussed in the next section. From the structure function, it is possible to indirectly derive the power spectrum, $\Phi_n(\kappa)$, that serves as the atmospheric model for this research. The power spectral density is a measure of the quantity of eddies with sizes $\frac{2\pi}{\kappa}$. The Kolmogorov spectrum describing the index fluctuations within the inertial subrange is

$$\Phi_n(\kappa) = 0.033 C_n^2 \kappa^{-\frac{11}{3}} \quad , \quad \frac{1}{L_o} \ll \kappa \ll \frac{1}{l_o}. \tag{8}$$

This spectrum, however, is only accurate within the inertial subrange. When used, it is assumed that the inner scale is zero and the outer scale is infinite to account for all frequency components [1:53]. However, when the inner and outer scales cannot be ignored, a more complete model is necessary. The modified spectrum, based on the Hill spectral model, not only addresses the inner and outer scales, but is modified to fit temperature data collected in the atmosphere [3]. This model is generally accepted in representing a generic atmosphere with common turbulence characteristics. It is the model used in this research and is given by

$$\Phi_n(\kappa) = 0.033 C_n^2 \left[1 + 1.802 \left(\kappa/\kappa_l \right) - 0.254 \left(\kappa/\kappa_l \right)^{7/6} \right] \frac{\exp\left(-\kappa^2/\kappa_l^2 \right)}{(\kappa^2 + \kappa_o^2)^{11/6}} \quad , \quad 0 \le \kappa \le \infty , \tag{9}$$

where $\kappa_l = \frac{3.3}{l_o}$ and $\kappa_0 = \frac{1}{L_o}$. This power spectrum is significant in that it is used to generate phase screens to load to the SLM. The atmospheric model can be tailored by selecting appropriate inner scale, outer scale, and path integrated C_n^2 values depending on the laser beam propagation scenario including turbulence strength. C_n^2 depends on height above ground (h in meters). Its value is found by integrating $C_n^2(h)$ over the path that laser light would travel to the sensor. To accomplish this task, the Hufnagel-Valley (H-V) model is chosen describing $C_n^2(h)$. Like the modified spectrum for the atmosphere, the H-V model is most commonly used for generic conditions describing $C_n^2(h)$, as it is based

11

on real data of various seasons, altitudes, and geographic locations [1]. The H-V model used is

$$C_n^2(h) = 0.00594(v/27)^2(10^{-5}h)^{10}\exp(-h/1000) + 2.7 \times 10^{-16}\exp(-h/1500) \\ +A\exp(-h/100) \quad , \quad (10)$$

with v as the root-mean-square wind speed in (m/s) and A as the value of $C_n^2(0)$ at the ground in $m^{-2/3}$. Specifically, the H-V$_{5/7}$ model is used corresponding to $v = 21\,m/s$ and $A = 1.7 \times 10^{-14}\,m^{-2/3}$. These values yield an $r_o = 5\,cm$ and an isoplanatic angle of $7\,\mu rad$. These choices for v and A are normally chosen for generic turbulence.

In summary, the atmospheric model used for this research has several components. The power spectrum of index of refraction variation, $\Phi_n(\kappa)$, is the atmospheric model. It originates from the index of refraction structure function, $D_n(R)$, and is based on real-world data. Two components of the power spectrum control its behavior. These components are the inertial subrange (l_o, L_o) and the structure constant C_n^2. Furthermore, the structure constant is an integration over the path length of laser light to the sensor and is height dependant based on the H-V$_{5/7}$ model. From the atmospheric model, phase screens are created to load to the SLM.

Atmospheric Identifiers. Several benchmarks exist to verify system behaviors based on the input atmospheric model. Two basic identifiers are the phase structure function and the intensity distribution. The structure function, mentioned above, can be inferred by measuring the resultant phase from the SLM over many screens with the same atmospheric statistics. The atmospheric model above (Equation 9) has roots in the Kolmogorov structure function. This structure function is used as the standard to evaluate the spatial light modulator's phase manipulation. The Kolmogorov structure function depends on the coherence length r_o. The coherence length is the size of an aperture diameter that gives the best image in a system looking through a particular portion of the atmosphere. Any increase in diameter above r_o collects more light, but does not provide increased resolution because of the aberrations caused by the atmosphere.

In evaluating system performance in producing atmospheric perturbations, a known benchmark concerning intensity is used called the lognormal distribution. This intensity distribution is given by

$$p(I) = \frac{1}{2\sqrt{2\pi}I\sigma_\chi} \exp\left[-\frac{\left(\ln\frac{I}{A^2}-2\langle\chi\rangle\right)^2}{8\sigma_\chi^2}\right] \quad, \quad I > 0 \ , \tag{11}$$

where I is the intensity, A is the unperturbed field's amplitude, and σ_χ and $\langle\chi\rangle$ are parameters of the distribution. The mean and variance of the lognormal distribution are

$$\begin{aligned}\mu_I &= \exp\left(\langle\chi\rangle + \frac{\sigma_\chi^2}{2}\right) \\ \sigma_I^2 &= \exp\left(2\langle\chi\rangle + 2\sigma_\chi^2\right) - \exp\left(2\langle\chi\rangle + \sigma_\chi^2\right).\end{aligned} \tag{12}$$

The lognormal distribution stems from one classical theory of optical wave propagation called the Rytov approximation. It builds on small fluctuations in refractive index as multipliers to the unperturbed wave [1]. The lognormal distribution is accurate only in a "weak fluctuation" regime measured by the Rytov variance

$$\sigma_1^2 = 1.23 C_n^2 k^{\frac{7}{6}} L^{\frac{11}{6}}, \tag{13}$$

where k is the wave number and L is the path length. For the atmospheric model to exist in the weak fluctuation regime, its Rytov variance must be: $\sigma_1^2 < 1$ [4]. Therefore, in measuring the output intensity of the optical system under test, a lognormal distribution is expected with respect to the transverse location on the output plane over many phase screens. Comparing the resultant intensity distribution to the lognormal distribution assists in quantifying system performance.

2.4 Phase Screen Generation Theory

Modeling the atmosphere using knowledge of the sensor scenario and power spectrum allows phase screens to be produced to represent the atmospheric random process. These phase screens can then be loaded onto the spatial light modulator to affect light in the desired manner. Several methods exist for producing phase screens using the power

spectrum. Two predominant methods involve using the Zernike polynomial basis set to produce phase screens and using the inverse Fourier transform of a power spectrum with Gaussian random variables to produce phase screens. The Fourier transform method is more desirable for this research because of its ability to match a square screen implementation with the square layout of the SLM. One disadvantage in the Fourier transform method is that for simulations over longer time periods, an increasingly large screen must be computed. Additionally, the Fourier transform method produces screens that lack low frequency accuracy. In other words, the modified spectrum contains a large percentage of power in the low frequency components. In taking the inverse Fourier transform, these low frequency regions are allocated the same number of samples as the high frequency regions, so that low frequencies are underrepresented. To alleviate these two problems, a modification to the Fourier transform method is used called the "generalized Fourier series method [5]."

To facilitate understanding the Fourier series method, the power spectrum must be discussed in relation to random processes. Intuitively, the power spectrum of a random process is the average amount of power in each frequency component composing the random process. For this case, the random process is phase variation induced by the atmosphere. The power spectrum is related to the covariance of the phase variation, $B_n(R)$. Specifically, the power spectrum is the Fourier transform of the covariance given by

$$\Phi_n(\kappa) = \int\limits_{-\infty}^{\infty} B_n(R) e^{-j2\pi\kappa R} dR, \tag{14}$$

Equation 14 is known as the *Wiener-Khintchine theorem* [6]. The random process describing phase variation in the atmosphere is always real, so the covariance is a real and even function. Taking the Fourier transform of a real and even function yields another real and even function ($\Phi_n(\kappa)$ in Equation 14 above).

Starting with the modified power spectrum representing the atmosphere, it is possible to sample the power spectral density (PSD) at a fast rate in the low frequency region and give fewer samples to the high frequency region. In this way, the frequency regions that have a larger weight are sampled more often. The PSD is then randomized using

14

Gaussian variables with the appropriate variance. The result is an array of complex coefficients describing the frequency composition of a phase screen iteration. The complex coefficients exhibit circular complex Gaussian statistics with a variance corresponding to the previously sampled PSD. All that remains is to sum sinusoids of varying weights to produce the desired phase screen. Implementing this procedure is accomplished by the inverse Fourier series given by

$$\phi_k(x,y) = \sum_{n=-\infty}^{\infty} \sum_{m=-\infty}^{\infty} \mathbf{c}_{n,m} e^{j2\pi(f_{x_n}x + f_{y_m}y)}, \tag{15}$$

where (x,y) are spatial coordinates of the screen, $\mathbf{c}_{n,m}$ are randomized complex coefficients from the PSD of interest, and (f_{x_n}, f_{y_m}) are spatial frequency components from the PSD. The PSD's imaginary terms are zero because the covariance is real and even. By randomizing the PSD using a circularly complex Gaussian random variable, complex coefficients $\mathbf{c}_{n,m}$ are created containing a random phase. Therefore, each phase screen iteration $\phi_k(x,y)$ is unique and possesses a unique random phase in the Fourier domain.

An advantage in this method appears for applications requiring a sequence of screens to represent longer time periods (several seconds). Instead of calculating one large phase screen and moving the area of interest around the screen as time progresses, it is only necessary to calculate the screen exactly where it is needed. Although the generalized Fourier series method cannot take advantage of fast Fourier transform algorithms, calculations are still saved by only calculating the screen area of interest. To implement the Fourier series method, a PSD for the turbulence of interest is calculated using l_o, L_o, r_o and the spatial frequency region of concern. r_o comes from the path integrated C_n^2 found using the H-V$_{5/7}$ model. The relationship between C_n^2 and r_o is

$$r_o = 2.1(1.46k^2 C_n^2)^{-3/5}, \tag{16}$$

where k is the wave number. The Fourier series coefficients are then calculated for frequency components of interest (calculating more low frequency components). Afterward, the coefficients are used to construct the phase screen by summing sinusoids with differ-

ent weights at any location desired. Matlab code used to create screens can be found in Appendix A.

2.5   Phase Modulation

For this research, realizing phase screens must be accomplished in a quick and adaptive way to enable the testing of varied atmospheric conditions. The spatial light modulator (SLM) is capable of implementing sequences of phase screens for this application. It operates by sending electronic signals to an array of electrodes to dictate the amount of phase delay experienced by light passing through it.

In this work, a phase-only light modulator built by Boulder NonLinear Systems is used. As light passes into the device, it is reflected by an array of electrode mirrors and then exits the device. In entering and exiting, the phase of light is delayed by a nematic liquid crystal (NLC) layer. The amount and location of the delay on the incident light is controlled by the array of electrode mirrors. Figure 2 shows a cross-section of the SLM and the path that light follows. Light travels through the top three layers, reflects from the electrodes, and passes through the top three layers a second time. The first layer is a
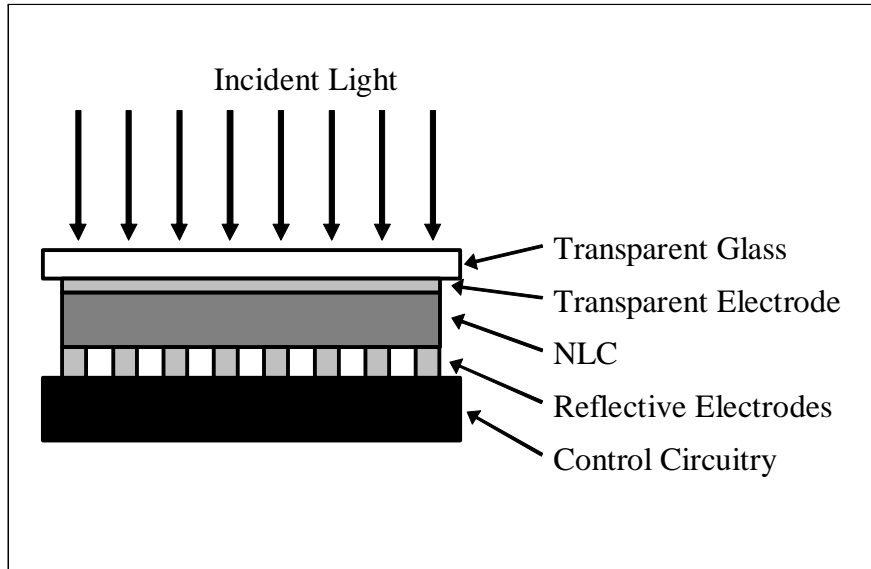
Figure 2   SLM cross-section with incident light entering and exiting from top layer

glass substrate with a transparent common electrode deposited on it. Immediately after

16

this is a layer filled with NLC. Behind this layer, a 512×512 array of reflective electrodes is deposited on a second substrate layer. These electrodes have a dual role to reflect light passing through the system and emit an E-field that manipulates the NLC.

NLC is the active element in the SLM and consists of molecules that behave as crystal molecules do; they form regular geometric latices. These molecules are also free to move as in a liquid phase and can change physical orientation together in the whole lattice. "Nematic" identifies the property that the molecules tend to orient themselves in the same direction, but not in ordered layers. This common orientation is due to the cigar-like shape of the NLC molecules [7]. The dielectric anisotropic property of the NLC allows the molecules to be manipulated by an externally applied E-field. This E-field affects a change on the physical orientation of the molecules. Figure 3 shows a typical layout of NLC with its orientation marked as the director. Because of the birefringent properties
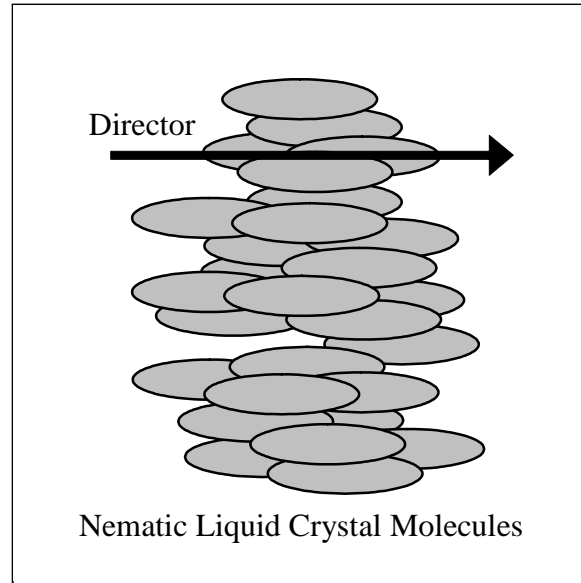
Figure 3   Nematic liquid crystal director marked horizontal

of the crystal, the index of refraction experienced by light passing through the material is variable depending on the polarization of the light. Light polarized perpendicular to the director sees an ordinary index of refraction. Light polarized otherwise sees a index that depends on an angle θ between the director and the direction of light propagation and is

described by

$$\frac{1}{n_e^2(\theta)} = \frac{\cos^2\theta}{n_o^2} + \frac{\sin^2\theta}{n_e^2}, \tag{17}$$

where n_e is the extraordinary index of refraction, n_o is the ordinary index of refraction, and $n_e(\theta)$ is the effective index experienced by the light [8]. If θ is 0° (polarization is parallel with the director), the crystal's birefringence ($\Delta n = n_e(\theta) - n_o$) becomes 0. For this condition, a strong E-field must be applied. At the other extreme of 90°, the birefringence is at its highest. Ideally, light incident on the NLC should be linearly polarized and parallel with the director when no e-field is applied. In this way, when an e-field is applied and the director rotates, the light ray still only sees one index of refraction (the extraordinary index $n_e(\theta)$). Therefore, the liquid crystal has a controllable index of refraction so that light passing through it experiences an optical path difference depending on the strength of the E-field across the NLC. The highest delay D in radians that can be experienced by the light is then

$$D = \frac{2\pi(n_e - n_o)l}{\lambda}, \tag{18}$$

where l is the thickness of the liquid crystal and λ is the wavelength of light [8]. Localized orientation changes can be effected on the NLC molecules by the reflective electrodes in the SLM. A specific voltage is induced across each electrode and the common transparent electrode to create an "image" of specified indices of refraction. In other words, a 512×512 element optical path difference map is created by the SLM so that incident light is delayed as dictated by the optical path difference map.

There are some issues to consider in regard to the SLM. The first is the small active area of each reflective electrode in the SLM. The reflective portion of each electrode only occupies 83% of each pixel on the SLM [9]. Therefore, space between each electrode exists that does not reflect light incident on the SLM. The configuration of this inactive space acts like a diffraction grating in which multiple orders of light are reflected from the SLM. This diffraction behavior means that light is reflected in multiple directions, forcing incident light to split into each of these directions. The amount of light in the first order (reflected light on the optic axis) is reduced, thereby lowering the optical efficiency of the system. A second issue is that the relationship between the voltage induced across an

electrode pair and the amount of resulting phase delay is nonlinear. This relationship will be explored in this research so that accurate phase screens can be realized.

2.6 Wavefront Sensing

A Shack-Hartmann wavefront senor is used in this research to detect and verify correct system operation. The wavefront sensor measures the wavefront of light (the E-field phase) reflected from the SLM. It is not possible to directly measure the phase of light in the same way that one would measure the magnitude (actually magnitude squared). Instead, a wavefront sensor treats the incident light as many different samples which are individually analyzed.

To understand wavefront sensor functionality, consider a simple optical system with an aperture and a lens to focus light at a distance behind the lens as in Figure 4. If a plane wave parallel to the aperture is incident on the system, the intensity pattern observed is a spot on the optic axis of the system as in the top of Figure 4. Similarly, if this same plane wave falls incident on the aperture at an angle (has some tilt), it produces a spot shifted in some direction proportional to the amount of tilt of the plane wave as in the bottom of Figure 4. The focal plane of this system consists of four intensity detectors arranged in a
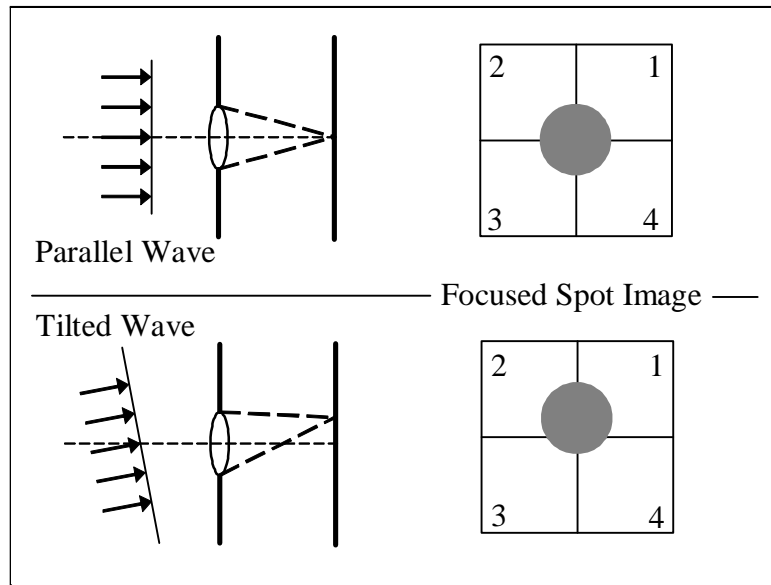
Figure 4   Light incident on lenslet of wavefront sensor

square, called a quad-cell. Tilt in the x direction is determined by averaging the left two detector intensities and subtracting from the average of the right two detector intensities. For the y direction, tilt is determined by averaging the top two detector intensities and subtracting the average of the bottom two detector intensities. Putting several of these systems side-by-side in an array produces a map of local tilt measurements in the x and y directions. These arrays can then be used to reconstruct the phase incident on the wavefront sensor. Measurements of the wavefront can then be compared to simulated results.

2.7 Simulation Theory

Simulation is referred to in this section in two ways. The first is that the optical system presented here is intended to simulate atmospheric effects on light. Arriving at a credible simulation using a relatively small SLM entails scaling a larger, real-world system to a small size. Second, simulating the optical system behavior (as on a computer) allows prior knowledge of system behavior and verifies correct operation of the system. Using computer resources, it is possible to implement actual equations and theories for realistic simulations.

System Scaling. System scaling is significant because the SLM being used has a height and length of only 7.68 mm. In addition, propagation for an in-door lab environment may only be one or two meters. In contrast, many optical systems operating in the atmosphere have an effective diameter of a quarter of a meter or more and propagate over kilometers. To compare optical systems of different sizes, the Fresnel number is often used. The Fresnel number is a parameter that relates wavelength λ, source aperture radius a, and propagation distance L and indicates the strength of diffraction effects due to propagation in an optical system. It is given by

$$F = \frac{a^2}{\lambda L}. \tag{19}$$

A large Fresnel number ($F > 1000$) indicates light propagation in a linear manner, whereas $F \ll 1$ indicates a strong influence of diffraction on light propagation and a Fourier transform can be used as in Equation 3 to calculate a field at a certain distance [2]. When

comparing two systems of unequal scale, it is important that the Fresnel number be similar for each system so that the effects of diffraction are nearly equal. In considering the size of an optical system, it is also important to account for turbulence strength. The most direct way of scaling atmospheric turbulence is through the coherence length r_o. In particular, by keeping the ratio of the source diameter to r_o constant, the system's behavior is preserved when scaling from one size to another. For example, suppose that an optical system with a source diameter of 25 cm operates in turbulence with an r_o of 10 cm, and that a simulation system with an aperture of 2.5 cm must be used to analyze the scenario. In order to obtain an accurate representation, r_o for the turbulence must be $(10\,\text{cm}/25\,\text{cm}) \times 2.5\,\text{cm} = 1\,\text{cm}$. These scaling concepts must be taken into account when converting from a real scenario to the small-scale lab simulation.

Computer Simulation. Computer simulation using wave optics code is necessary to understand and validate system behavior. Simulation is accomplished using Wavetrain. Wavetrain uses basic diffraction and propagation theory along with efficient computer algorithms to speed simulation calculation times. In the most basic sense, Wavetrain handles any optical system by ordering a sequence of light propagations and thin screen applications. Invariably, light propagation is the most computationally intensive element in an optical simulation. By taking advantage of the Fourier transform nature of the Fresnel integral (Equation 3) , the computations are greatly simplified. One failing of the Fresnel integral comes in the sampling of the wavefront at the end of propagation (the receiver plane). The sample spacing and extent of the wavefront (the amount that is calculated) is directed by the sample spacing and extent of the initial wavefront (the source plane). This situation is unacceptable in cases where it is too computationally expensive to implement the Fresnel integral using a large number of samples needed for the ending wavefront. Wavetrain handles this issue by allowing user specification of the sample spacing and wavefront extent. It then uses a two-step Fourier transform algorithm to compute the propagated wave. A minimum number of samples can be used to describe the wavefronts at either end of the propagation so that computational requirements are minimized. Having calculated a propagated wavefront, Wavetrain then applies the appropriate thin phase screen or amplitude screen to simulate different optical elements

or phenomena. The propagation/phase screen sequence repeats in the appropriate order until the simulation is complete.

Care must be taken in choosing the correct sample spacing and wavefront extent for initial and final wavefronts. One challenge is that a given wavefront can have dissimilar spatial frequency behavior in amplitude and phase, but only one sample period is used to adequately represent both amplitude and phase. The amplitude must be sampled at a minimum of two times the highest spatial frequency to satisfy the Nyquist criterion. At the same time, the phase must be sampled with a high enough frequency to ensure that the change from one phase sample to the next is not greater than π radians. Phase representation is modulo 2π when using the Fresnel Integral. For this reason, phase changes that jump from one sample to the next by more than π can be misconstrued as, for example, an increase in phase from the first sample to the next, when in reality, a decrease in phase occurred. Setting the physical extent of the grid that describes the field also affects the accuracy of the simulation. The grid size at the output plane after a propagation must be large enough to represent all light incident on the plane. It must also be large enough to avoid frequency wrap around affects caused by the Fourier transform algorithm used to propagate the light. Specifically, if λ is the wavelength of light and dx is the sample period used to represent the field, the diffraction angle of light exiting one sample point is $\frac{\lambda}{dx}$. If the propagation distance is z, the light from one sample point covers a length at the output plane of $\frac{\lambda z}{dx}$ [10]. The above relationships can be used to formulate a rule for choosing a sample period. Specifically, if prior knowledge exists about the size of the grid that one would like to observe at the receiver plane, a necessary sample spacing involves the length of both the source and receiver combined. So the sample spacing is

$$d_{xy} = \frac{\lambda z}{D_{source} + D_{receiver}}. \tag{20}$$

The grid size at the output plane should in general be $2\frac{\lambda z}{dx}$ to allow enough space to view the propagated light while not experiencing wrap-around effects from the Fourier transform used in the Fresnel integral [10]. Further, the diameter of the source can be related to the

previous expression to determine the necessary grid size

$$size_{grid} = D_{source} + \frac{\lambda z}{d_{xy}}, \tag{21}$$

where D_{source} is the diameter of the source and d_{xy} is the sample spacing chosen for the propagation. Equation 21 is a rule of thumb that may not guarantee absence of wrap-around if the propagation is over a large distance from a small source diameter.

With Wavetrain simulations of any optical system, the sample spacing, size, and number of points used to represent a propagated field can change throughout the system. To control the sample spacing and wavefront extent, an element named "Propagation Controller" must be inserted at the beginning or end of a propagation. Integrating the above rules into a system to execute an accurate simulation can take time, but allows consistent system behavior in a variety of scenarios.

2.8 Summary

Several theoretical concepts have been combined to enable the introduction of controllable atmospheric aberrations into an optical system. The primary concepts covered in this chapter necessary to enable the system are reviewed below:

- Propagation of coherent light pertinent to the aberrating system of interest is predicted with great accuracy by the Fresnel integral. The Fresnel integral consists of a Fourier transform of a known wavefront with an added quadratic phase factor. These two elements serve to simplify computation of the propagated wavefront. This knowledge is essential for system simulation and verification.

- Atmospheric turbulence is described using theory on the variation of index of refraction. A structure function describing this variation leads to the atmospheric power spectrum that serves as the atmospheric model. In turn, the power spectrum is used to create phase screens to control a spatial light modulator.

- Phase screens are generated from the power spectrum using the a generalized Fourier series method. By sampling the power spectrum more often at the low frequency

end, greater screen accuracy is achieved. These phase screens serve to implement atmospheric conditions for use in an aberrating system.

- Using nematic liquid crystal, a spatial light modulator induces a controllable phase delay on light. Once minor adverse effects of the SLM are compensated, phase screens are physically realized so that incident light wavefronts are manipulated as if they travelled through the atmosphere with identical properties.

- A wavefront sensor must be used to measure resultant aberrated wavefronts to verify system behavior. The sensor operates by using an array of lenslets to sample the wavefront and compute local tilts associated with each sample. The tilt data is then used to reconstruct a representation of the measured wavefront.

- To simulate real-world scenarios, optical system size scaling must be addressed. The Fresnel number identifies the degree of diffraction influence in an optical system. It is important that the Fresnel numbers of the real system and lab simulation nearly match. Also, the ratio of source diameter to coherence distance must be kept constant when scaling from one size to another.

- Using the same theory discussed in describing light propagation and atmospheric modelling, a software package called Wavetrain is capable of simulating the behavior of light in an optical system. This tool can troubleshoot anomalies of the designed system and verify correct system operation.

In the following chapters, the theory discussed here will be applied to design and operate a atmospheric aberrating system.

III. Methodology

3.1 Introduction

Using the theory of Chapter II to understand the atmosphere and how light interacts with it is necessary to build an optical lab-bench tool that manipulates a laser beam as would the atmosphere. The main tool designed consists of an optic bench with various elements including the spatial light modulator (SLM) and WaveScope camera. Additionally, computer interfaces exist to control the SLM, WaveScope, and imaging camera. This chapter describes a study of the SLM to map characteristics (mentioned in Chapter II) such as the nonlinearity between phase delay and pixel value. It also describes the procedure developed to operate the aberrating system and evaluate its performance.

3.2 SLM Configuration

Two issues must be resolved before using the system to obtain trustworthy results. First, the SLM response must be measured. That is, the amount of phase delay occurring for each gray value on a screen bitmap must be determined to insure that the SLM creates the correct phase modifications. In the SLM, birefringence of the liquid crystal splits the light into an ordinary (unaltered) component and an extra-ordinary (altered) component. The term "delay" is used to describe the distance measured between the ordinary and extra-ordinary light components for a snap-shot in time taken after the light has exited the SLM. In this discussion, delay will have units of radians. To convert from meters to radians, delay is multiplied by $\frac{2\pi}{\lambda}$. To measure the phase response of the SLM, an optical setup is used so that light from the SLM undergoes an amplitude change along with a phase change. With the addition of amplitude attenuation, the light intensity is measured and related to phase delay. Figure 5 shows the modified optical setup that achieves phase and amplitude modulation.

The modified optical layout contains a polarizer oriented to pass vertically polarized light from the laser. A polarizing beam splitter is oriented to reflect vertically polarized light to the left toward the SLM. A half-wave plate is added between the polarizing beam splitter and the SLM. The targetboard is moved to the exit side of the polarizing beam
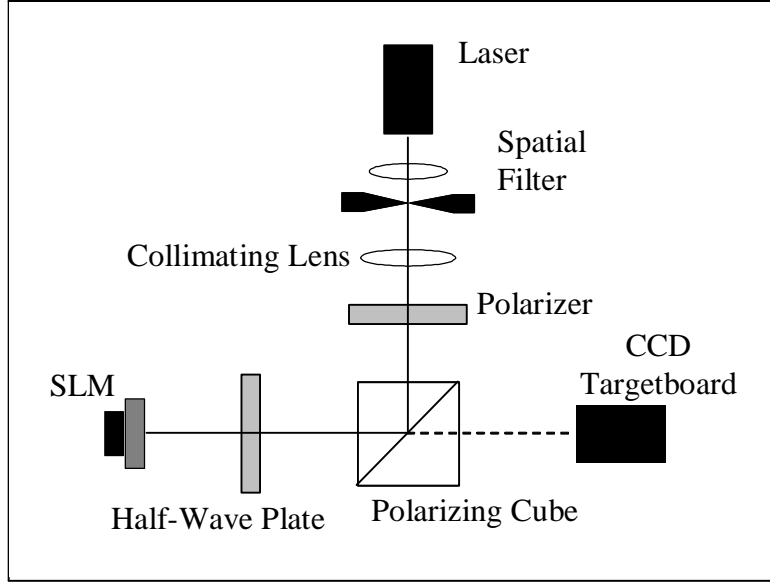
Figure 5   Modified optical layout with polarizing elements

splitter to pick up light from the SLM. In this setup, vertically polarized light from the laser enters the beam cube and is reflected toward the half-wave plate. This plate rotates the linearly polarized light to exactly $45°$ from the LC director (measured in the plane containing the SLM face) when no E-field is applied to the SLM. The SLM then delays the light (phase modulation) and changes the linear polarization to some degree of elliptical polarization depending on the E-field applied to the SLM.

To better understand this phase and intensity modulation, two cases are discussed. First, consider the case where an SLM E-field is applied with a potential difference of 1.38 V. Vertically polarized light travels from the laser source to the polarizing cube where it is reflected toward the SLM. The half-wave plate rotates the vertically polarized light by some angle. The light contacts the SLM and is not altered because the liquid crystal director has been rotated so that it is perpendicular to the linear polarization of the light (only ordinary light exists). Also, the polarization is unchanged by the SLM. The half-wave plate rotates the light back to vertical polarization so that it is reflected by the beam cube away from the camera, resulting in a minimal intensity at the camera.

Second, consider the case where an E-field from a 1.99 V potential difference is present on the SLM. Vertically polarized light travels from the laser source to the polarizing cube

26

so that it is reflected toward the SLM. The half-wave plate in front of the SLM rotates the polarization. Light then makes contact with the SLM so that its polarization is exactly $45°$ from the SLM director. At this point, mostly all the light is delayed (becoming the extra-ordinary component) by half a wavelength in the SLM. The polarization remains linear, but gets rotated by $90°$. Now, the half-wave plate rotates the light to the horizontal position. Light is then passed by the polarizing cube to the camera to achieve a maximum intensity (see Figure 6).

Outside these two cases (minimum and maximum intensity), the polarization is modified by the SLM to some degree of elliptical polarization. The output intensity at the camera is dependent on the amount of vertically polarized light that contributes to this elliptical polarization. The amplitude behavior output from the SLM system is, therefore, described by

$$A = \sin\left(\frac{Delay}{2}\right), \tag{22}$$

where delay has units of radians. So, the phase delay in radians is related to the intensity attenuation by

$$Delay = 2\sin^{-1}(\sqrt{I}), \tag{23}$$

where I is normalized between zero and one. To calibrate the SLM, a series of solid-gray bitmaps is loaded, each with a different gray value ranging from 0 to 127. Gray values from 0 to 255 are available but values 128 through 255 duplicate values 0 through 127 in reverse order as the liquid crystal molecules do not respond to the polarity of the E-field. The resulting average intensity over the entire targetboard is recorded for each image. These intensities are then normalized between zero and one. The results are shown in Figure 6. The intensity response tends to flatten out toward SLM value 127 in Figure 6. This phenomenon is most likely due to the non-linear rotation of the liquid crystal molecules with decreasing E-field. Equation 23 is then used to convert intensity to phase delay. Measured results are in Figure 7.

From this point, the region from 0.4 to 1.4 waves is chosen to represent phase screens. In this region, 256 gray values are mapped to 127 SLM values to represent phase delay in a linear fashion. A custom lookup table is created to load the proper SLM value

27

SLM Intensity Response
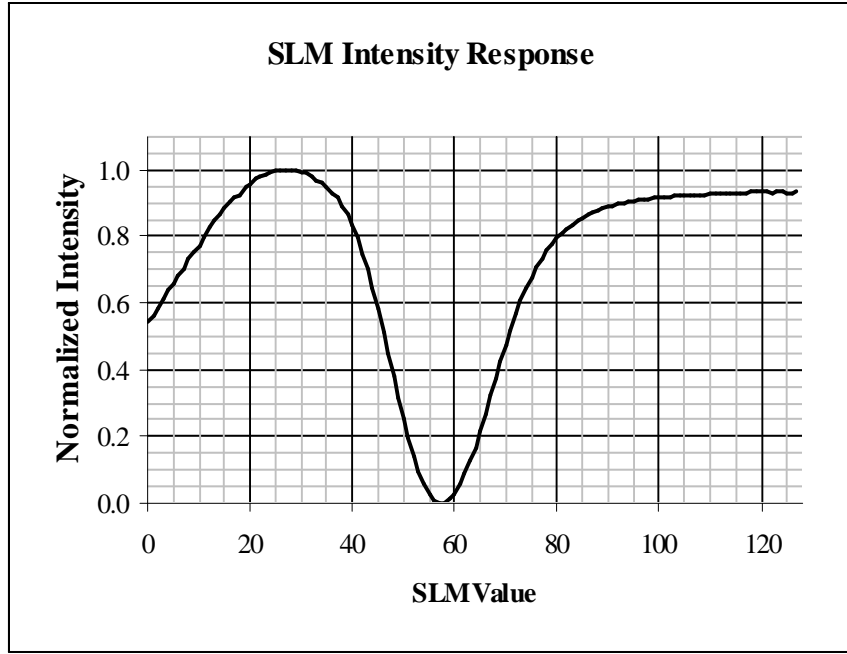
Figure 6   Normalized intensity results of solid gray images from 0 to 127

that corresponds to the desired phase delay value of a given screen.   The lookup table translates phase screens using gray values of 0 to 255 to phase delay values from 0 to 2π. By measuring the phase delay response of the SLM to gray values, loaded screens are correctly represented.

Another issue comes from the geometry of the SLM. Each pixel on the SLM array has a fill factor of only 83%. Non-reflective area exists between each pixel. The result is a diffraction grating that reflects light into multiple orders (or directions), each containing only a percentage of the intensity of the incident beam. The zero order diffraction contains only 65% of the total power reflected from the SLM. A larger problem exists when collecting intensity pattern information for a given turbulence screen loaded on the SLM. Intensity at the zero order diffraction spot interferes with the intensity patterns created by turbulence screens.   Since interference from the zero order diffraction is unique to each screen, it is difficult to compensate for the zero order diffraction by adding a correcting phase to each screen or by post processing the intensity capture to remove the interference.   Instead, the intensity from the turbulence screen is steered by the SLM away from the zero order diffraction area, which is accomplished by adding a constant tilt phase to each turbulence

28
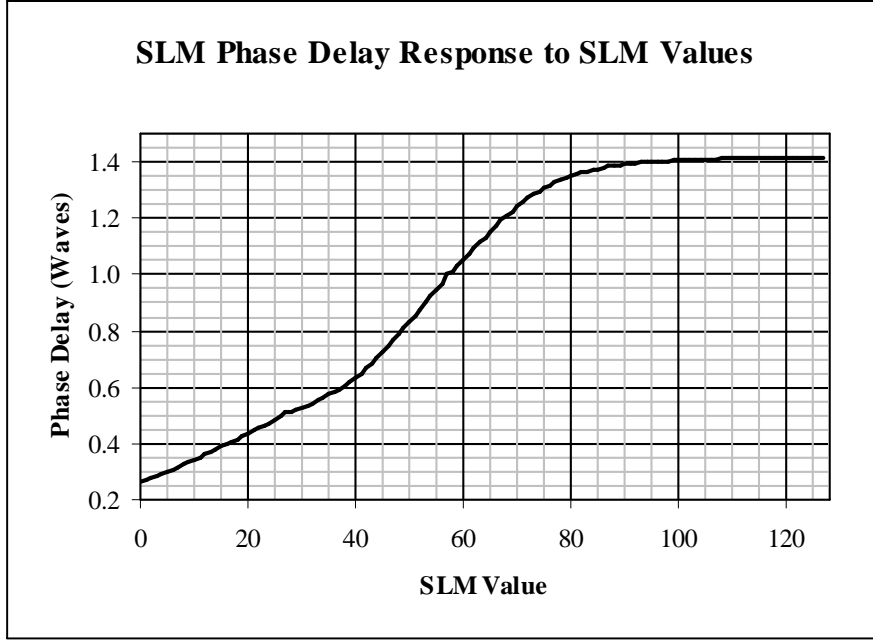
Figure 7   SLM values correspond to phase delay

screen.   For the propagation distance of 770 mm from the SLM to the targetboard, the
beam is steered by 14.1 μrad using a tilt of 95 waves each in the x and y transverse
directions, or 134 waves in the diagonal direction.   Figure 8 shows the resulting output
with the beam steered down and to the right from the more faint zero order diffraction spot
in the top left. The SLM represents phase delay modulo 2π, so the tilt screen used to steer
the beam acts as a diffraction grating as well. Thus, 63.7% of the power contained in the
original zero order diffraction with no tilt screen is present in the steered beam as a result of
the tilt diffraction. Fewer waves of tilt could have been used to steer the beam away from
the zero order, but intensity variations are greater when using fewer waves of tilt as a result
of the 2π modulation. An example of this intensity variation is shown in Figure 9. Here,
134 waves of tilt create the more uniform intensity shown in Figure 10. In summary, the
83% fill factor and diffraction behavior require steering the beam by 14.1 μrad from center
axis.   Using 134 waves of tilt keeps a uniform intensity pattern so that when turbulence
screens are added to this tilt, their intensity patterns are not further changed. According
to the Nyquist sampling criterion, there is a maximum spatial frequency that the SLM
can represent. Based on two samples per period and the SLM pitch of 15 μm, the spacial

29

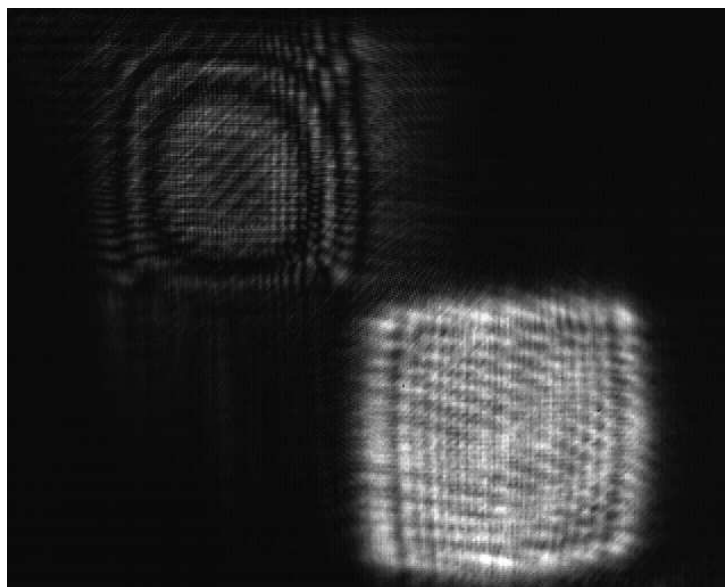Figure 8   Steered beam using a tilt screen to avoid interference by zero order diffraction
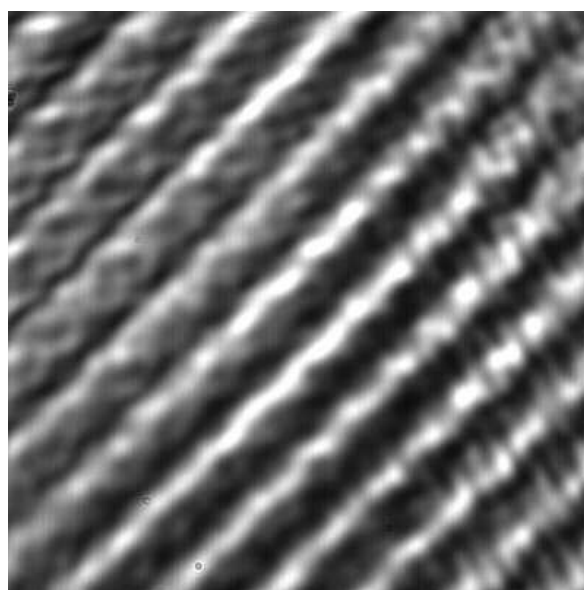
Figure 9   Intensity pattern close-up resulting from a tilt screen, demonstrating 35 waves of tilt
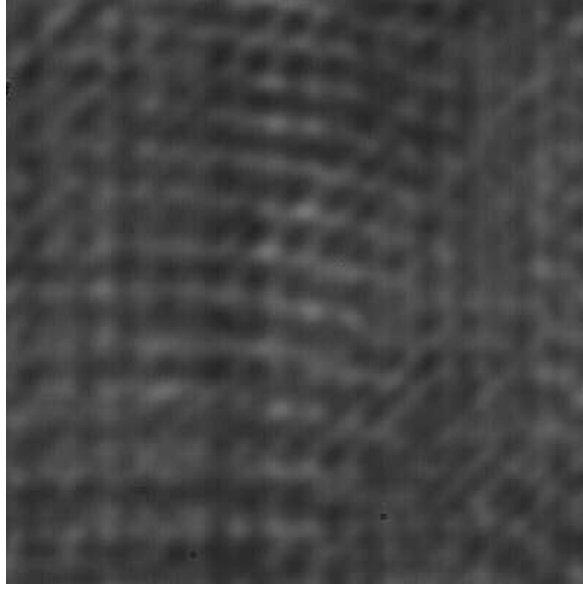
Figure 10   Intensity close-up of 134 waves of tilt resulting in a more uniform intensity
behavior than with 35 waves of tilt

frequency limit is $3.33 \times 10^4 \, \text{m}^{-1}$ in both the x and y directions (with respect to the lab

bench system size, not the propagation scenario size). With 134 waves of tilt added to

each screen (or 95 wave in both x and y directions), the maximum spatial frequency left

available in both x and y directions is $2.10 \times 10^4 \, \text{m}^{-1}$. The highest spatial frequency with

the strongest turbulence case tested (see Chapter IV for test cases) is $9.9 \times 10^3 \, \text{m}^{-1}$.

3.3   Optic Bench Layout

Attention must be given to the optical setup of the aberrating system to understand

its operation. The experimental system shown in Figure 11 consists of simple optical

elements, the SLM, and the WaveScope camera. A Helium-Neon laser beam operating

at $3 \, \text{mW}$ and $632.8 \, \text{nm}$ is directed into a spatial filter consisting of a $60 \times$ objective lens

focused onto a $10 \, \mu\text{m}$ pinhole. The spatial filter focuses light from the laser at the exact

position of the pinhole. The result is an approximate point source. A lens with $F\# \, 0.75$

then collimates the light. The column of light passes through a 50/50 beam splitter, of

which one beam (the reference beam) falls incident on a mirror flat. The other beam (the

test beam) falls on the SLM with a loaded phase screen. A beam dump is used to block

31
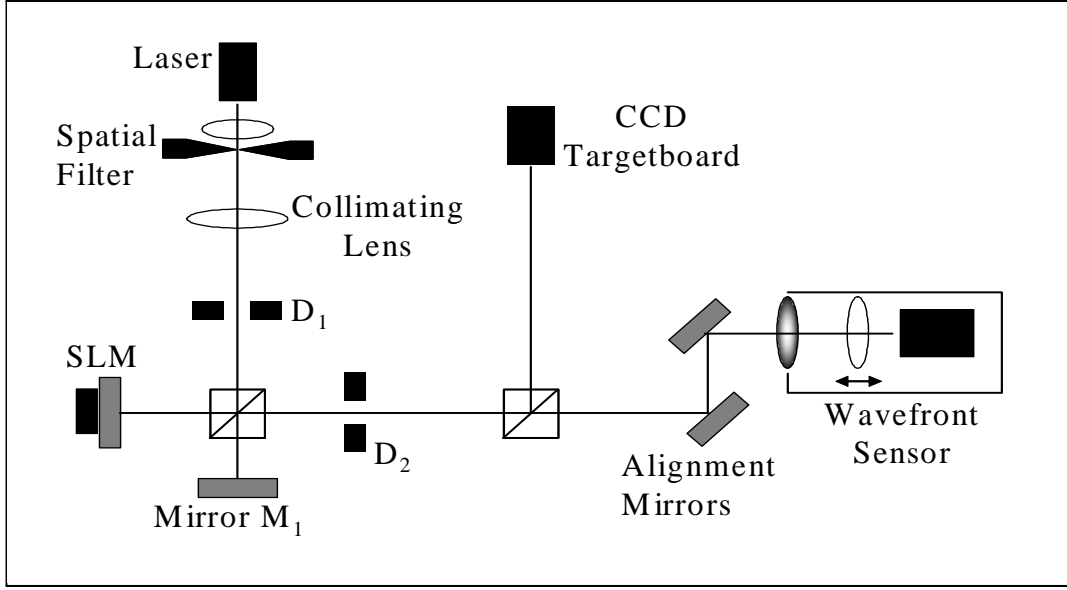
Figure 11   Optical diagram of aberrating system

either the reference or test beam, thereby allowing only a single beam to move on to the cameras. The selected beam passes through the beam splitter a second time and on to a targetboard and the Shack-Hartmann wavefront sensor via a beamsplitter.

Two personal computers are used in the experiment. The first interfaces to the wavefront sensor using a parallel port cable for transfer of control signals and an RCA cable for direct video feed. Software on the computer controls exposure levels and performs all calibration routines for proper operation of the wavefront sensor. The wavefront sensor is a WaveScope 2.0 package from Adaptive Optics Associates, Inc. The front of the wavefront sensor holds the lenslet array. Three separate arrays provided with the system have lenslet pitches of $480\,\mu$m, $300\,\mu$m, and $133\,\mu$m. The $300\,\mu$m pitch array (MLM300S) is used to sample the output wavefront for this experiment. The second computer controls the SLM and targetboard. The SLM user interface is capable of configuring a sequence of images and loading them onto the SLM. The lookup table is loaded here to convert 256 gray values to appropriate SLM values for proper phase delay behavior. The targetboard is a CMOS Ultra camera by Computer Modules, Inc. It has a 1280×1024 array of $7.5\,\mu$m pitch. The device has its own software for capturing images and setting up various configurations.

3.4   System Operation Procedure

Lab Bench System.   To operate the system, a phase screen is produced using the Fourier series method in Matlab. The phase screen in the form of a bitmap is loaded onto the SLM with the Blink software. Light passes through the system to the cameras. A capture of the resultant intensity pattern is saved as an image file from the targetboard and a phase measurement is saved from the wavefront sensor. The process is repeated for each phase screen loaded onto the SLM. For each scenario, 100 screens are sequentially loaded and results are recorded for the wavefront sensor. Since the phase screens are 512×512 pixels, each iteration of a phase screen is advanced by 512 pixels in both the x and y directions so that each screen is completely new. 200 screens are created for each scenario for intensity measurements. Here, the screens are advanced only 6 pixels in the x and y directions so that a continuous progression of intensity is captured. With 200 screens, over two completely new screen periods are cycled.

Computer Simulation.   Simulating the lab bench system on a personal computer is accomplished using Wavetrain. Details for operating this software can be found in Appendix B. Using Wavetrain's graphic user interface, a simplified aberrating system is setup with various optical elements. Parameters such as wavelength, propagation distance, aperture diameter, and sample size are defined for the system. The SLM is represented as an optical path difference in meters, followed by a square aperture to attenuate the light that extends around the optical path difference map. All dimensions match as closely as possible to the lab bench setup. Figure 12 shows the Wavetrain system.

3.5   Summary

Two issues with the SLM cause undesired effects in the atmospheric simulator system. The first is the non-linear phase response of the SLM to gray values. This issue is resolved by measuring the response and creating a lookup table for the SLM that maps gray values to phase delay in a linear fashion. The second issue is the 83% fill factor, which creates a diffraction screen behavior where the zero order interferes with the intensity pattern of interest. Therefore, the beam with the intensity pattern of interest is steered off the optic

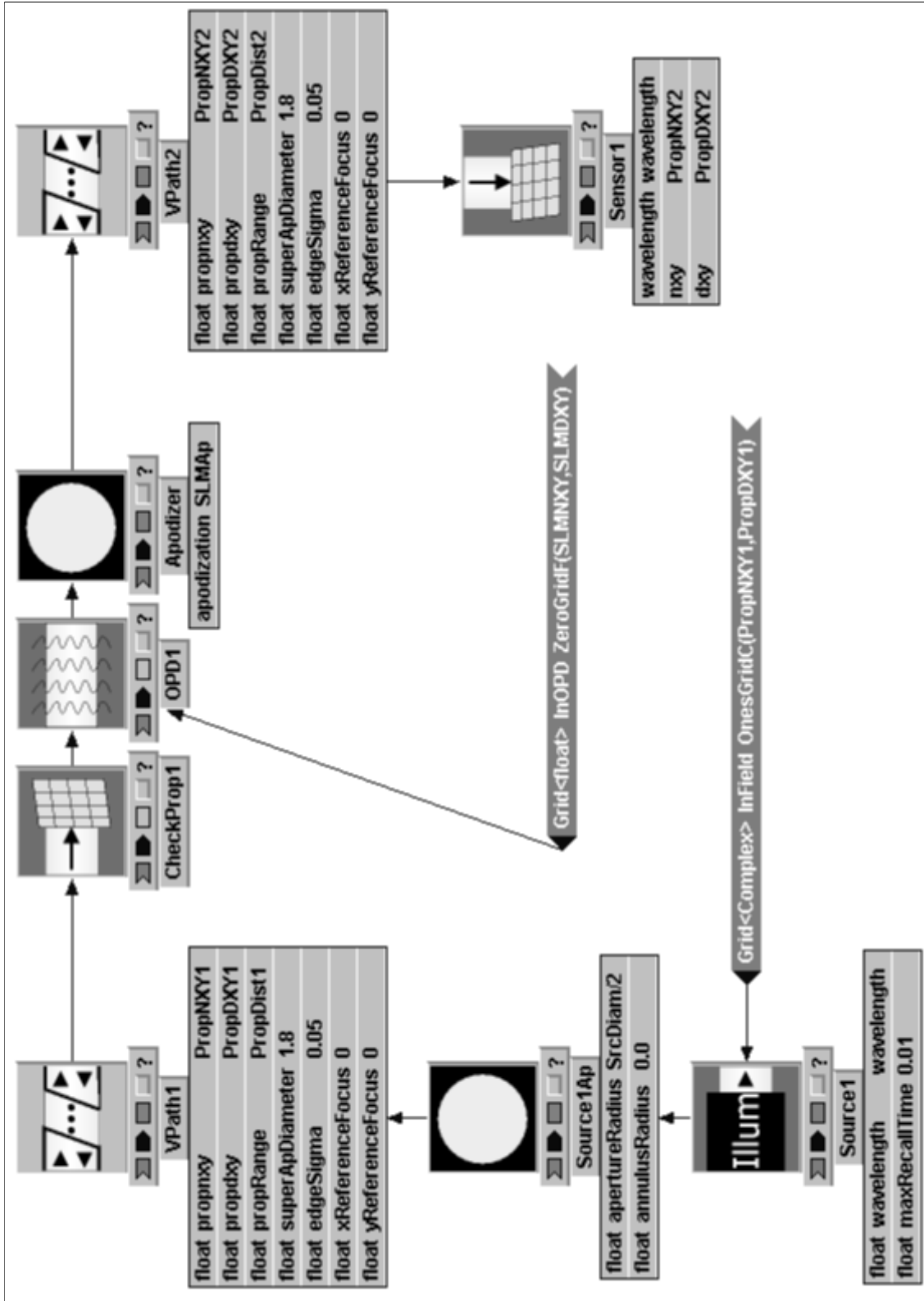Figure 12   Wavetrain simulation of aberrating system (light propagates from bottom-left to bottom-right)

34

axis using a tilt screen of 95 waves in both the x and y directions. Simulating atmospheric aberrations is then be accomplished by loading phase screens to the SLM with a tilt added to each screen. Intensity data and phase data are then collected by the cameras and wavefront sensor respectively.

IV. Results and Analysis

4.1 Introduction

Atmospheric simulation is achieved using the optical system described in Chapter III. The ability of this system to duplicate real world atmospheric effects is dependant on the atmospheric phase screens and the spatial light modulator's ability to represent those screens. Validating the system is, therefore, accomplished by investigating the phase screens themselves and evaluating the product of the spatial light modulator (SLM) over various turbulence scenarios. Five scenarios are chosen for laser propagation through turbulence that involve low altitude aerial engagements, a high altitude engagement, and a ground to high altitude engagement. Each scenario represents a real-world possibility where laser energy is directed at an aircraft. Following the scenario description, a quantitative evaluation of system scaling is necessary to classify the aberrating system's closeness to real scenario sizes. Results of each scenario are then presented with emphasis on phase and intensity statistics so that an error analysis can be completed. Lastly, displaying Wavetrain simulations alongside system results help indicate acceptable behaviors.

4.2 Test Cases and Scaling

Based on common situations identified by the Air Force, five scenarios or test cases are created to properly demonstrate the aberrating system's ability across a range of turbulence strengths. Each case is identified by a starting altitude where the laser source is located, an ending height where the target aircraft operates, and a propagation distance from source to target. Table 1 identifies each test case.

Name	Start Alt. (m)	End Alt. (m)	Prop. Distance (m)	Source Diam. (cm)
Case 1	12000	12000	100000	25.4
Case 2	10	5000	5000	25.4
Case 3	10	1000	2000	25.4
Case 4	10	10	1000	25.4
Case 5	10	10	2000	25.4

Table 1   Test scenarios used in aberrating system

Name	D/r_o **Ratio**	**Real** r_o **(cm)**	**Lab System** r_o **(cm)**	**Fresnel Number**
Case 1	2.88	8.79	0.265	0.255
Case 2	3.71	6.85	0.207	5.09
Case 3	6.74	3.77	0.114	12.74
Case 4	13.10	1.94	0.0586	25.48
Case 5	19.86	1.28	0.0386	12.74
Lab System	-	-	-	21.98

Table 2   Test case scaling attributes and Fresnel numbers

As established in Chapter II, a power spectrum called the modified spectrum serves as the atmospheric model to create phase screens. This model depends on the atmospheric coherence length r_o, which is calculated from the path integrated C_n^2 value using the Hufnagel-Valley profile. Once r_o is found, each case must be scaled to the size of the lab bench optical system. The reference to accomplish this scaling is the source aperture size. For each case, a source aperture of 25.4 cm corresponds to an SLM diameter and hence, a source diameter of 7.68 mm for the lab system. The coherence distance is scaled using the relationship found in the *System Scaling* section of Chapter II. Finally, the Fresnel number for each case and the lab system Fresnel number are computed. All scaling attributes are found in Table 2.

Several items of importance appear in Table 2. Fresnel numbers for the cases and the lab systems have low orders of magnitude indicating that diffraction plays a significant role in each scenario. Ideally, the Fresnel number of the lab system should closely match the Fresnel number of each case. Due to spacing requirements of certain optical elements on the lab bench and the difficulty of changing the system layout for each new case, the optics and propagation distances are left unchanged throughout the entire experiment. The lab system Fresnel number is an acceptable match to the case Fresnel numbers. Another trend apparent in Table 2 is the decreasing coherence length with each scenario, which is due to the altitude and propagation distances of each scenario. Longer propagation distances attenuate the coherence length because the path integrated C_n^2 increases. In general, lower altitudes also decrease coherence length because the C_n^2 profile generally contains higher values at lower altitudes. These trends are intuitive because turbulence increases in strength at lower altitudes and for longer path lengths.

4.3 Turbulence Screen Validation

Having quantified the test cases and system scaling, it is possible to validate the turbulence screens used to represent the atmosphere. For turbulence screen creation, a Matlab program is written to generate the power spectrum, sample it, and sum weighted sinusoids over a defined spatial axis. These screens are modulated over 0 to 2π to support the dynamic range of the SLM. 100 screens are created for each case where each iteration is a completely new screen. These screen sets serve to verify proper phase behavior. Additionally, 200 screens were created for each case to verify intensity distributions. Each set of 200 screens is sequenced such that from one screen to the next, the phase representation is scrolled by six pixels in both the x and y directions. When intensity measurements are taken (explained in the following section) it is desirable to view the intensity correlation of points in close proximity to each other. Moving the screen by only six pixels in the x and y directions benefits the intensity measurements. Specifically, the intensity distribution will compare more closely to the log normal distribution. An unmodulated sample screen is shown for each case in Figures 13 through 17.
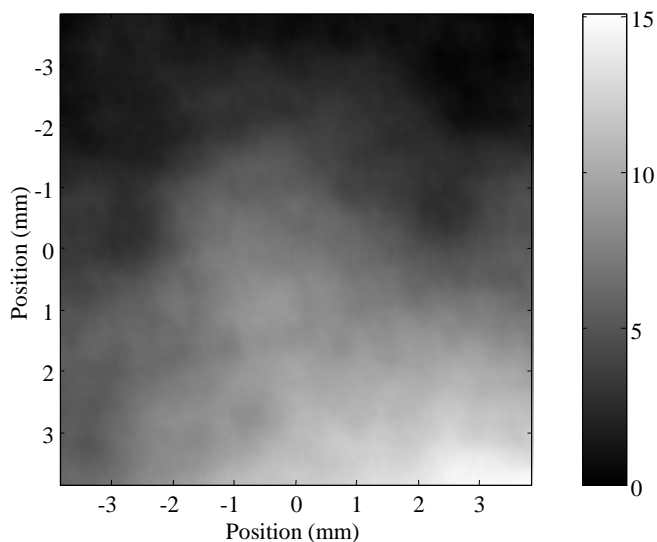
Figure 13   Case 1 sample phase screen in radians (weak turbulence)

Progressing from Case 1 to Case 5, a noticeable increase in optical delay is present, portrayed by the range bar to the right of Figures 13 through 17. This increase matches
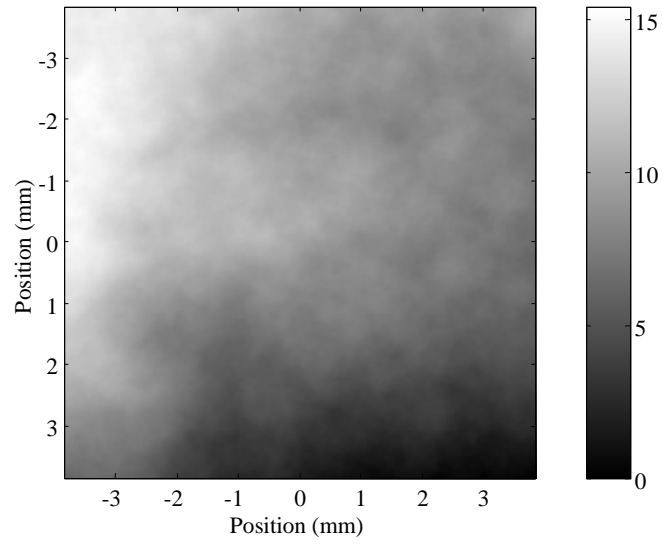
Figure 14   Case 2 sample phase screen in radians
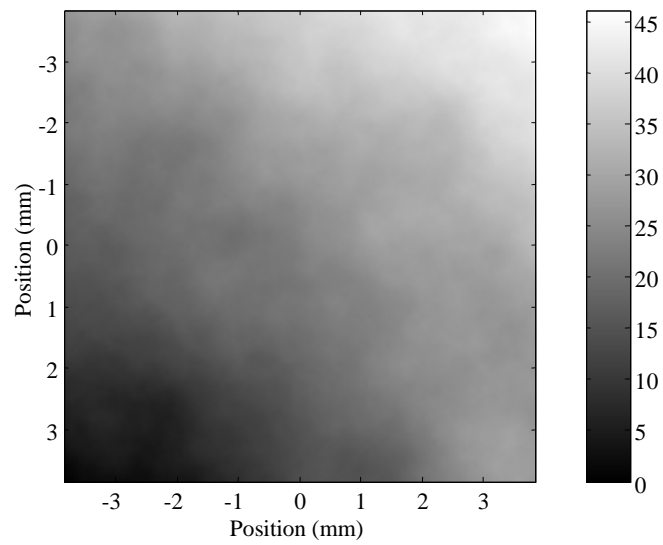
Figure 15   Case 3 sample phase screen in radians
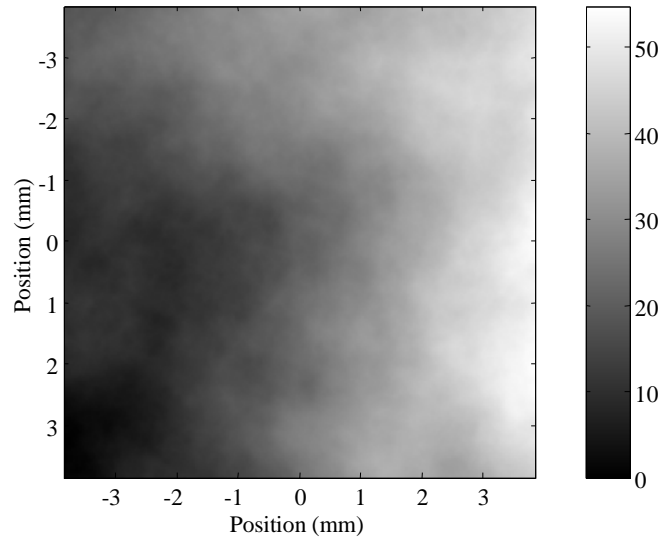
Figure 16   Case 4 sample phase screen in radians
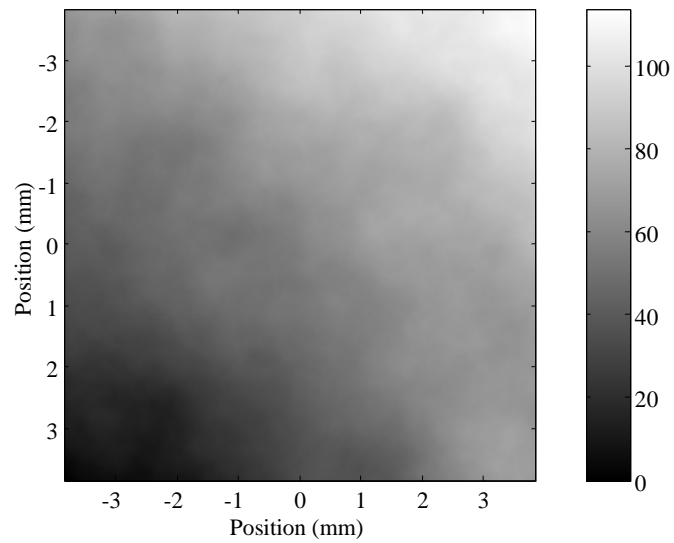
Figure 17   Case 5 sample phase screen in radians (strong turbulence)

with the decrease in coherence length over Cases 1 through 5. Unfortunately, these screens cannot be validated with a rudimentary comparison of optical delay. Instead, the structure function of each screen is determined and compared to the theoretical Kolmogorov structure function given by Equation 7 in Chapter II. The definition of the structure function (Equation 5 in Chapter II) is implemented in Matlab over 100 screen iterations to obtain a measure for each turbulence case. The average structure function over 100 trials is then plotted with the Kolmogorov structure function for comparison. The results for each case are in Figures 18 through 22. The average percent error between the Kolmogorov
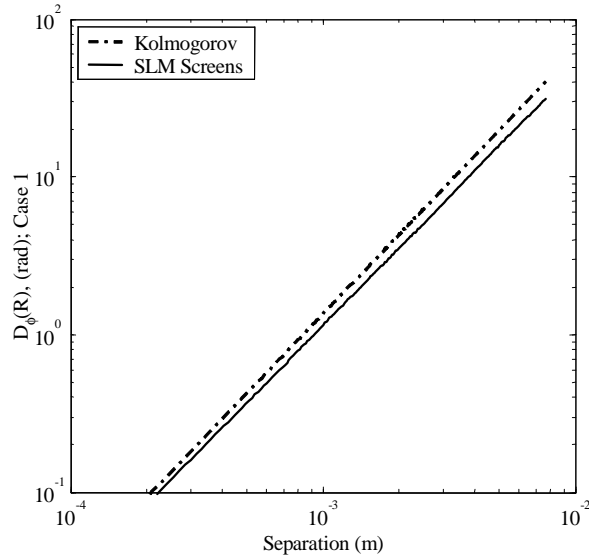

Figure 18   Case 1 SLM screen structure function comparison to Kolmogorov theory

and calculated structure functions for Cases 1 through 5 are: 18.8%, 5.3%, 3.5%, 5.0%, and 3.6%, respectively. This error depends slightly on the random number draws used to randomize the coefficients of the set of screens created by Matlab. It also depends on the number of power spectrum samples used to create the screens; more samples help to reduce this error. For each case, 512 samples are taken from the atmospheric power spectrum models. In sampling the spectrum, a logarithmic scheme is used to favor low frequency components. In Figures 18 and 19, a slight dip in the screen structure function is apparent. This anomaly results from inadequate sampling of low frequency areas in the power spectrum. A more custom sampling scheme, or simply more samples could be

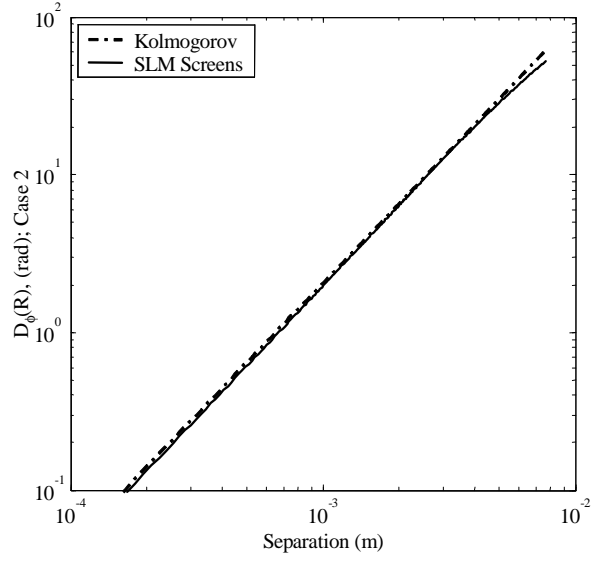Figure 19   Case 2 SLM screen structure function comparison to Kolmogorov theory
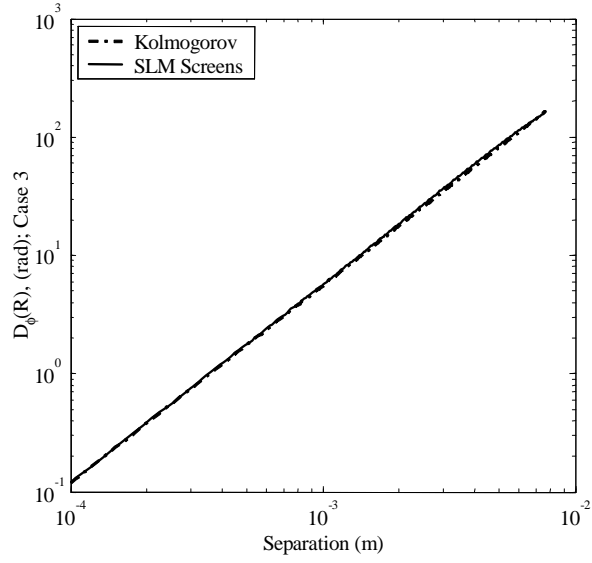

Figure 20   Case 3 SLM screen structure function comparison to Kolmogorov theory
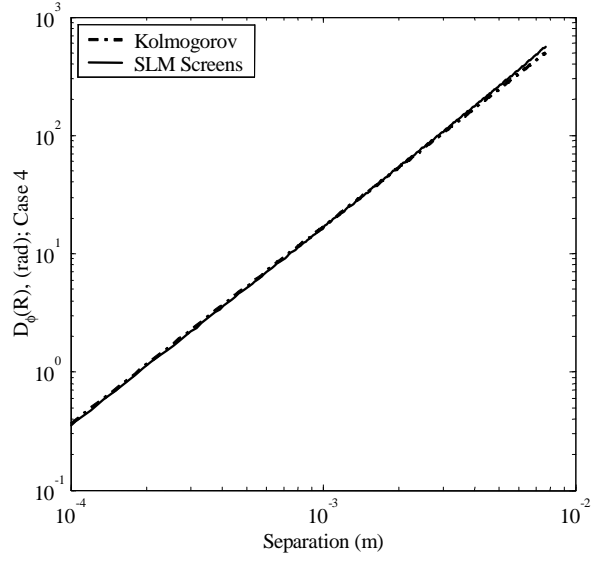
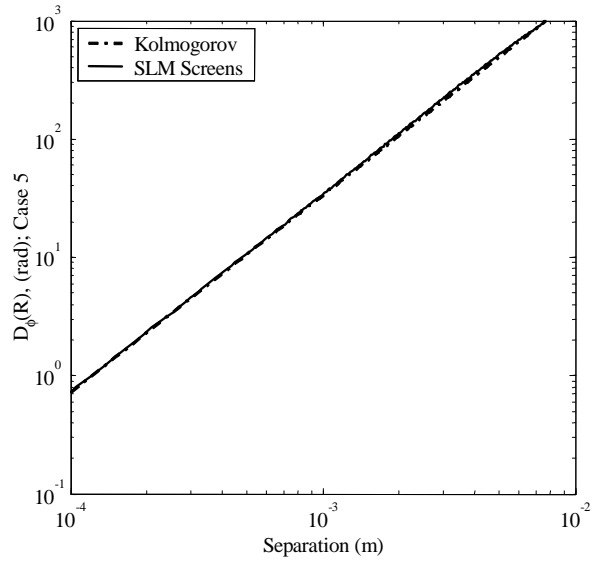Figure 21   Case 4 SLM screen structure function comparison to Kolmogorov theory

Figure 22   Case 5 SLM screen structure function comparison to Kolmogorov theory

used to improve this behavior. Overall, the screens exhibit structure functions that are acceptably close to the expected Kolmogorov theory.

4.4 Data Evaluation

Screens loaded to the SLM are shown to be near the predicted theory with respect to their structure functions. The data output from the lab bench atmospheric simulator is now analyzed to validate system behavior. In this experiment, two forms of data are collected: the phase of light outgoing from the SLM is reconstructed by the wavefront sensor, and intensity images are recorded by the CCD targetboard from light leaving the SLM. As mentioned in Chapter II, two analysis methods verify acceptable system operation. First, the structure function of measured phases is computed and compared to the Kolmogorov structure function (as above). Second, the intensity images are surveyed to obtain an intensity distribution with respect to a certain transverse location. These distributions are compared to the lognormal distribution governed by the weak fluctuation regime.

Phase Evaluation. For each of the five turbulence cases, 100 measurements are taken using the wavefront sensor. Phase reconstruction is performed by the wavefront sensor software to enable computation of the structure function. Figures 23 through 27 show structure function results compared to Kolmogorov theory. In each case, measured structure functions resemble the Kolmogorov theory. For Cases 1 through 5, the average percent error is 26.6%, 23.9%, 25.6%, 15.7%, and 32.0%, respectively. Several trends are apparent in these figures. Cases 1, 3, and 4 have structure functions that are higher than theory for small separation distances and lower than theory for large separation distances. A combination of two error sources most likely creates this behavior. First, a non-ideal calibration in the wavefront sensor may be present. For calibration of the wavefront sensor, a constant phase with no tilt is necessary. There may have been some tilt when the wavefront sensor was calibrated that adds to the turbulence wavefronts when taking measurements. This fault raises the entire structure function above the Kolmogorov theory. The second error source most likely comes from sensor limitations. Software controlling
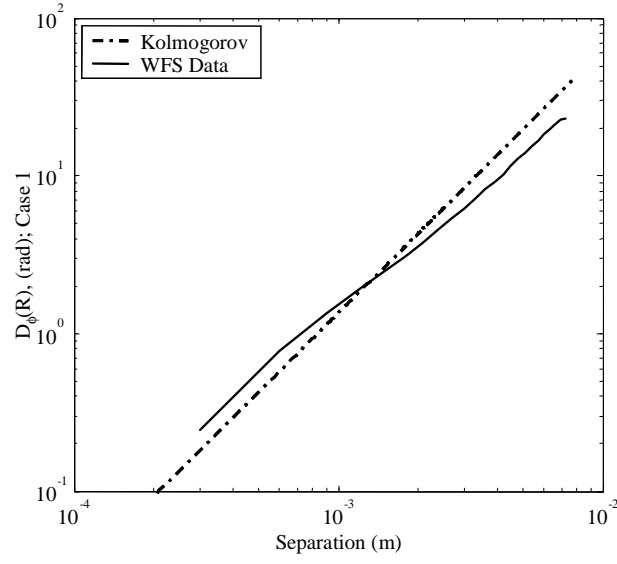
Figure 23   Case 1 structure function from wavefront sensor measurement compared to Kolmogorov theory
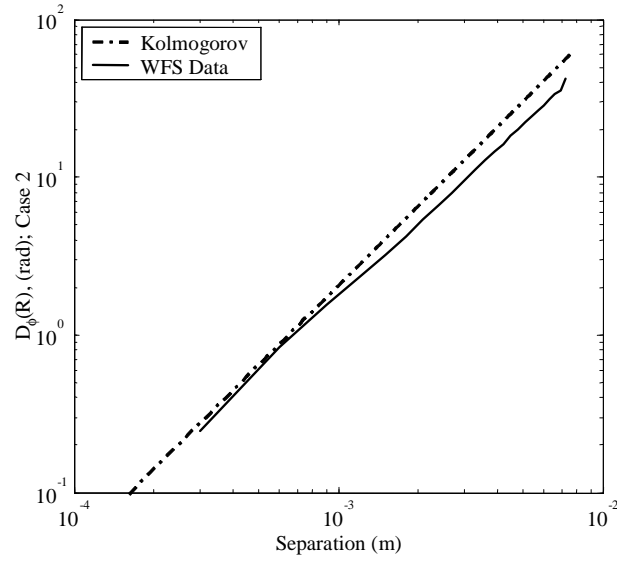
Figure 24   Case 2 structure function from wavefront sensor measurement compared to Kolmogorov theory

45
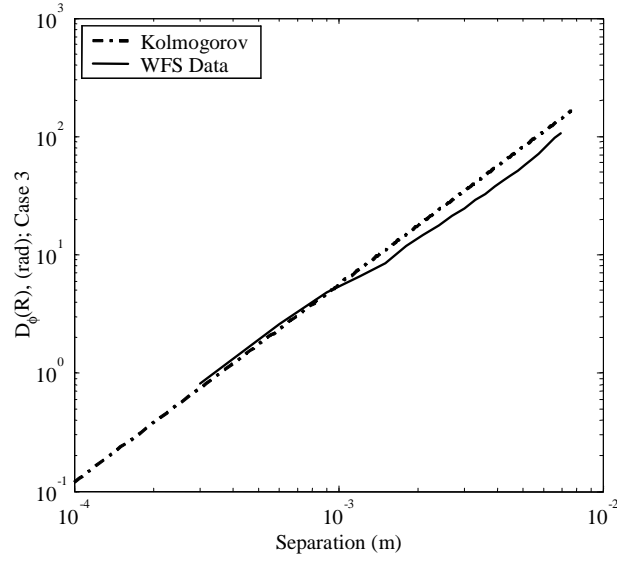
Figure 25   Case 3 structure function from wavefront sensor measurement compared to Kolmogorov theory
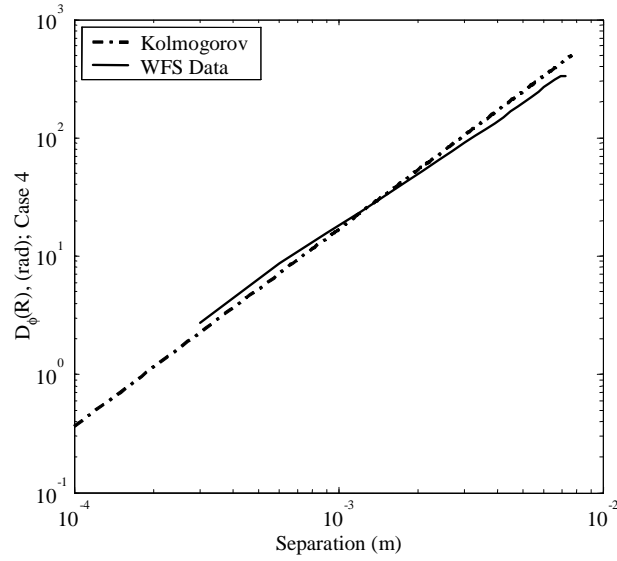
Figure 26   Case 4 structure function from wavefront sensor measurement compared to Kolmogorov theory
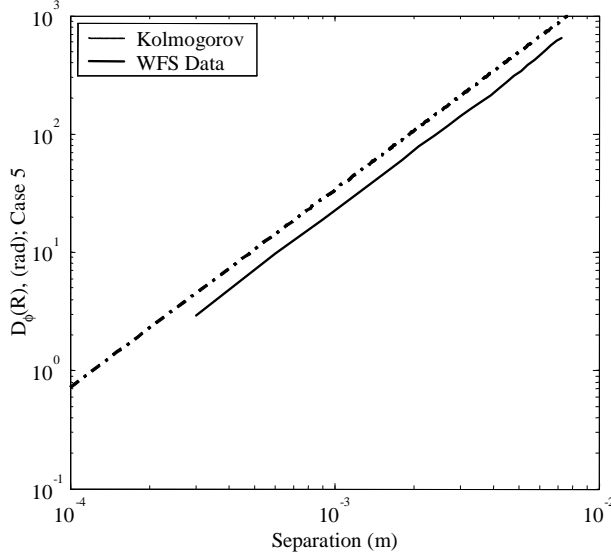
Figure 27   Case 5 structure function from wavefront sensor measurement compared to
              Kolmogorov theory

the wavefront sensor chooses when the intensity of a particular sample is too low to read an
accurate tilt measurement. In recording each system output, some samples near the edge
of the wavefront sensor field of view regularly have low intensity values.   These samples
are rejected and not incorporated in the phase reconstruction.   Larger separation dis-
tances depend on these outlying samples. When a sample is rejected, the large separation
distance measurement for the structure function is lost, and fewer iterations are averaged
for that particular separation distance.   The result is a decreased structure function at
higher separation distances. This large separation distance behavior is observed in Cases
1 through 4 (Figures 23 through 26).   Two positive aspects are that the measured data
is monotonically increasing and each case nearly maintains a 5/3 power relationship in r.
With respect to structure functions, the atmospheric simulator produces average quality
results over weak to strong turbulence.

    Intensity Evaluation.   Intensity is used to evaluate the atmospheric simulator as
well.   For each case, 200 screen iterations are loaded and their corresponding intensity
patterns are recorded by the CCD targetboard.   Figures 28 through 32 show sample
intensity patterns from Cases 1 through 5 (weaker to stronger turbulence). As expected,

47
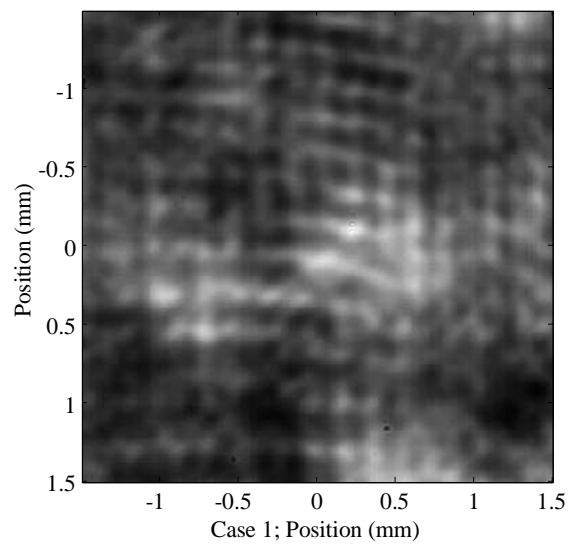
Figure 28   Case 1 sample intensity measurement
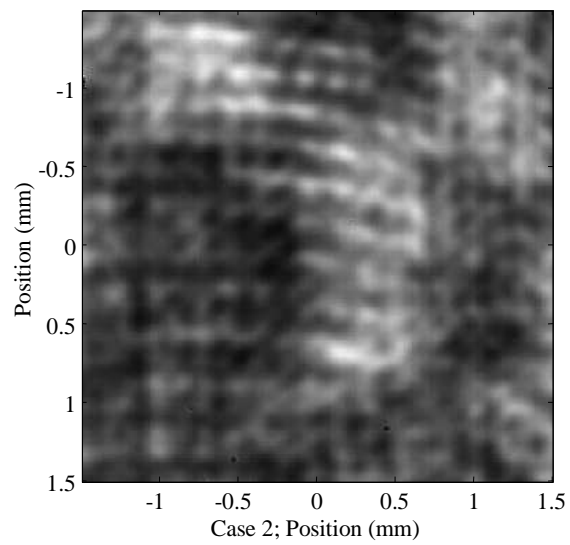
Figure 29   Case 2 sample intensity measurement
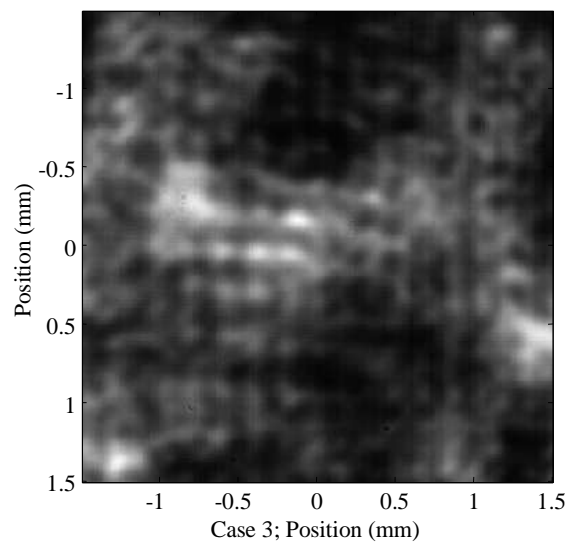
Figure 30   Case 3 sample intensity measurement
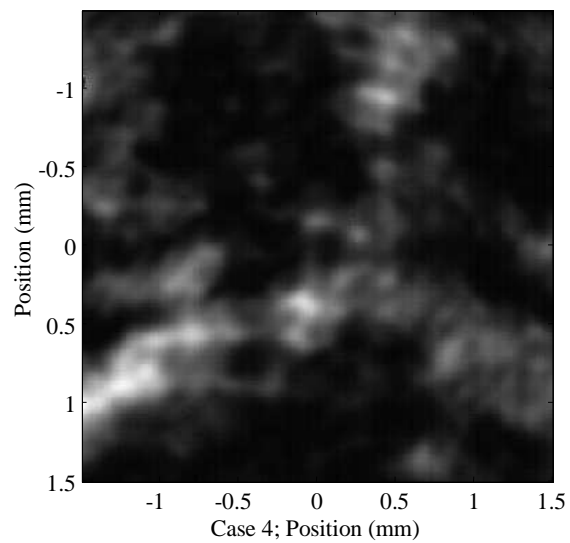
Figure 31   Case 4 sample intensity measurement

49
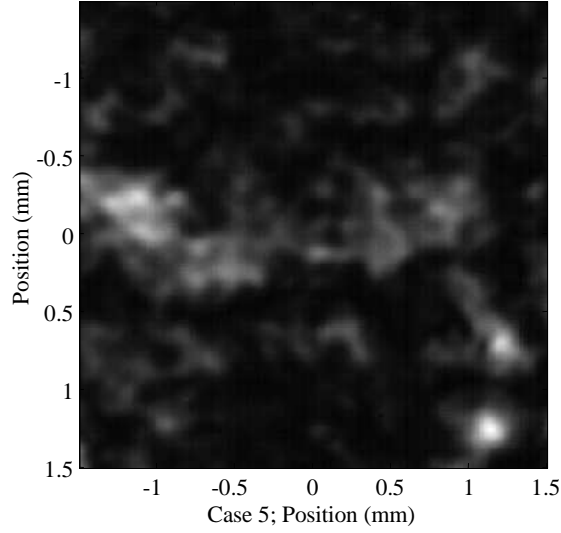
Figure 32   Case 5 sample intensity measurement

Case	Integration Time (ms)
1	14.56
2	13.94
3	8.53
4	4.58
5	4.37

Table 3   Targetboard integration times for each Case

weaker turbulence creates a more uniform intensity pattern. Stronger turbulence leads to more abrupt intensity changes and smaller areas of high intensity. In Figures 29 through 31 a cross-hatching or striped pattern is noticeable. These patterns are a combination of diffraction through the square aperture of the SLM and possibly interference fringes due to the glass protective layer on the CCD targetboard. Case 4 and Case 5 reveal faint or no cross-hatching because the increasingly varied phase overpowers aperture diffraction and interference. In collecting intensity patterns for each case, the CCD targetboard integration time is adjusted to take advantage of the full range of gray values. The CCD targetboard operates with 8 bits, so 256 gray levels are available. The integration time is adjusted so that the maximum intensity value over an entire screen set for a given case is near the highest gray level (256). This integration adjustment can be thought of as an intensity normalization. Table 3 shows the integration time for each case.

50

Case	Rytov Variance	Mean	Variance	Mean Square Error
1	3.617	0.298	0.019	1.34×10^{-4}
2	0.450	0.253	0.016	3.32×10^{-4}
3	0.380	0.186	0.013	5.70×10^{-4}
4	0.968	0.089	0.003	1.16×10^{-4}
5	3.451	.088	0.005	1.88×10^{-4}

Table 4   Intensity related statistics for each turbulence case

Turbulence characterized by the Rytov variance as "weakly fluctuating" is expected to be log normally distributed. To verify this property, a single location for each screen set is observed with respect to its intensity. A probability distribution is created and compared to the log normal distribution having the same log normal parameters as the data. In other words, the mean and variance of the data are used to calculate parameters $\langle \chi \rangle$ and σ_χ that are used in describing the log normal distribution. Figures 33 through 37 show the results. Although there is a resemblance to the log normal distribution in
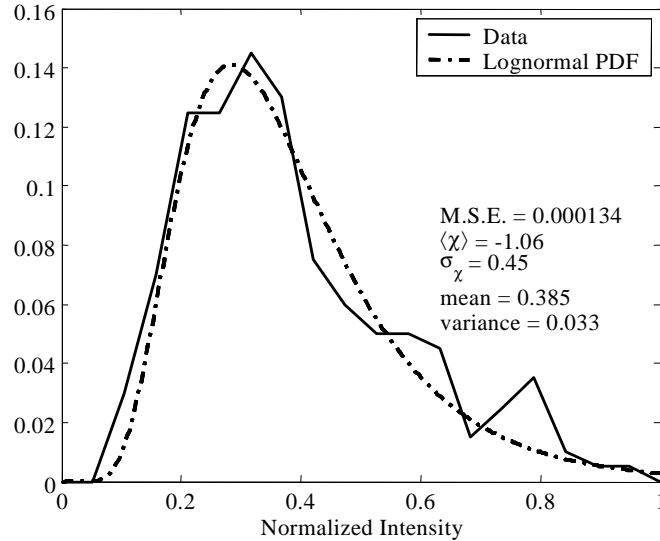
Figure 33   Probability distribution function for intensity of Case 1

Cases 1, 2 and 3, the data makes frequent departures from this standard. To help with explaining these behaviors, statistics and properties of each case are presented in Table 4.

Only Case 1 and 5 have a Rytov variance above 1, which puts these scenarios outside the weak fluctuation regime so (by Rytov's definition) the log normal distribution is no

51
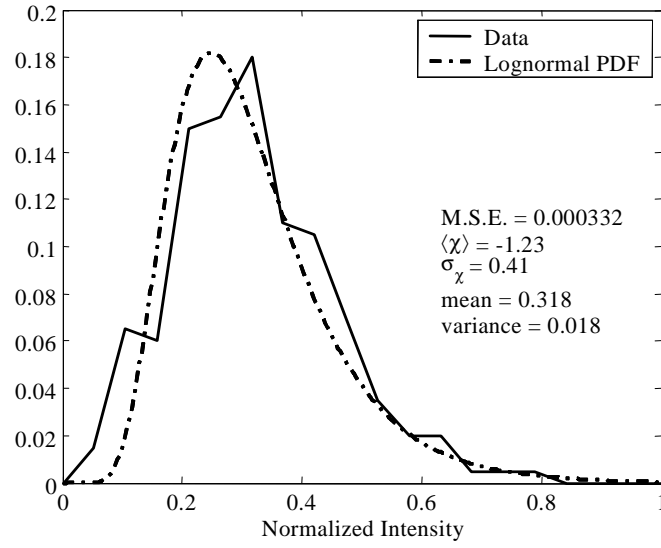
Figure 34   Probability distribution function for intensity of Case 2
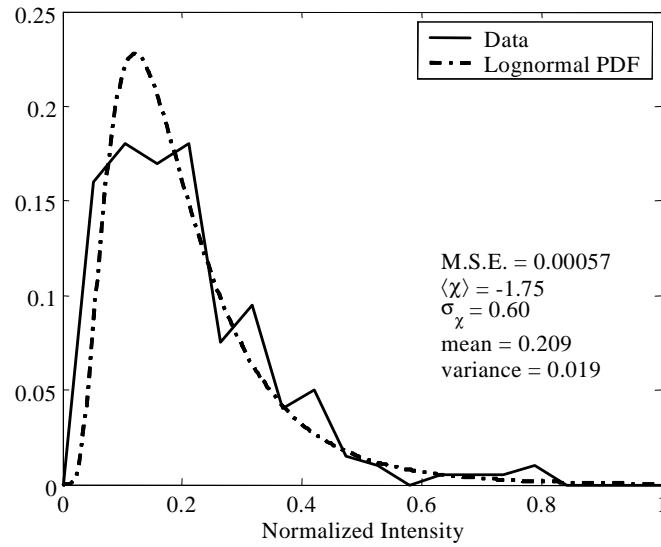
Figure 35   Probability distribution function for intensity of Case 3
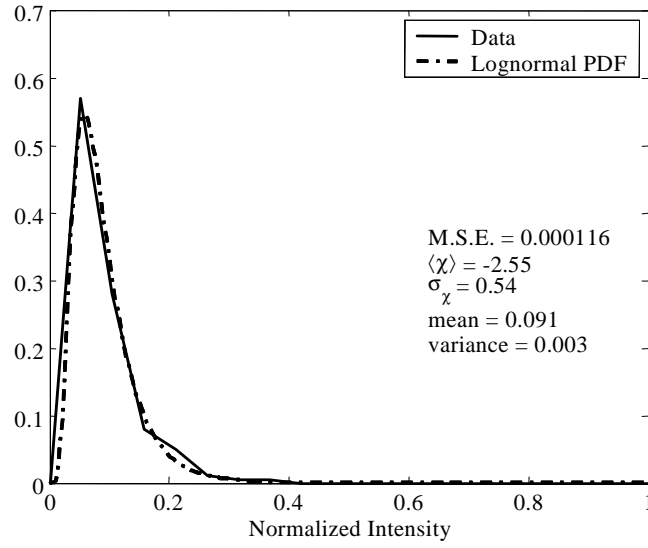
Figure 36   Probability distribution function for intensity of Case 4
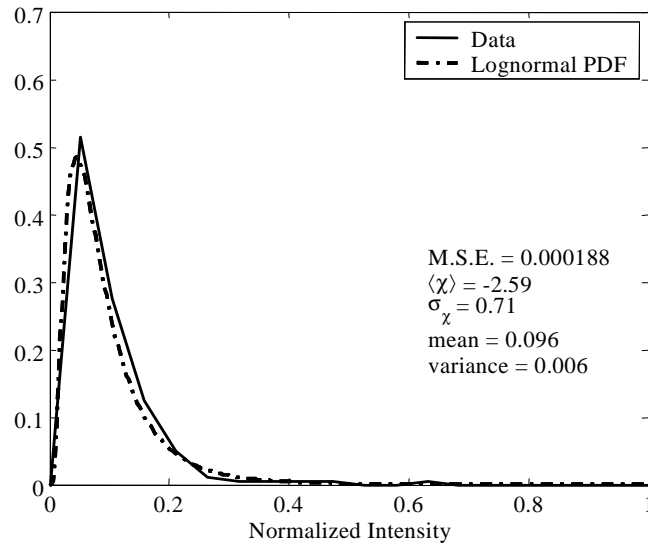
Figure 37   Probability distribution function for intensity of Case 5

longer an accurate prediction of the intensity distribution. Though outside weak fluctuation region, Case 1 has the second lowest mean square error. The log normal distribution can still be loosely applied to evaluate system operation here as well as in Case 5. In Case.1, 2, and 3, referring back to the intensity distribution in Figures 33, 34, and 35 helps explain the mean square errors. Diffraction patterns from the SLM aperture and interference from the CCD targetboard cover glass interfere with the turbulence effects on intensity. As the turbulence screen set is cycled through the experiment, diffraction from the SLM aperture is not stationary in location. Destructive interference areas due to the aperture tend to wander with, but not in the same manner as, the turbulence intensity patterns. In surveying a pixel location for a screen set, destructive interference distorts the true intensity value created by the turbulence screen. Additionally, the CCD targetboard facilitates viewing the complete turbulence intensity pattern, but its sensitivity to the incident light is not great enough to accurately measure intensity variation for weak turbulence. Therefore, error in Cases 1, 2, and 3 also stems from the CCD targetboard's limited sensitivity. Finally, measurement of the intensity distribution is an average of only 200 trials for each case. Increasing the number of trials would marginally improve measured results. A final comparison plot is shown in Figure 38. Here, all the log normal distributions are plotted together after equalizing the intensities using the integration times for each case. In stronger turbulence, the index variations create larger areas with low intensity. Further, light is more strongly focused at certain locations. Therefore, the mean and variance of intensity should decrease as turbulence is increased. This trend is verified in Table 4 and somewhat visualized in Figure 38.

Data in the from of intensity and phase measurements has been presented here to facilitate a judgement on whether the spatial light modulator is capable of creating accurate turbulence for laser warning system evaluation. Generated phase screens demonstrate good agreement with the Kolmogorov theoretical structure function. Screens for each turbulence case are, therefore, accurate representations of index of refraction fluctuations present in a turbulent atmosphere. Wavefront sensor measurements in the form of reconstructed phase maps are taken for each of the five turbulence cases. From these measurements, the structure function is calculated and compared to Kolmogorov theory.
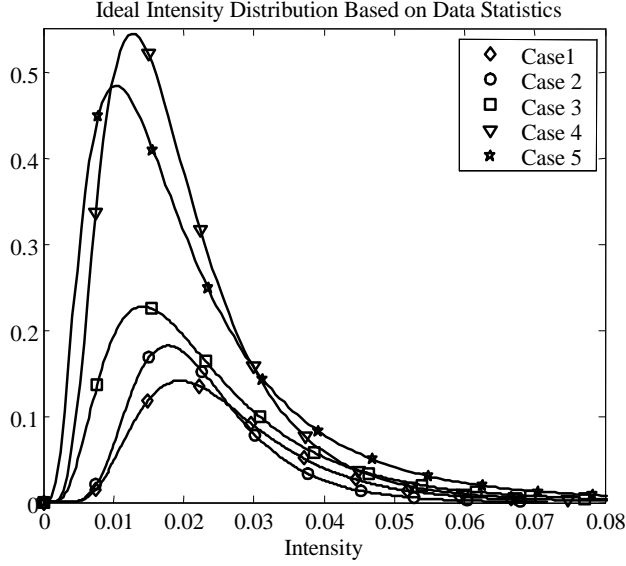
Figure 38   Comparison of log normal distributions calculated from data statistics for each set; intensity is a relative targetboard value

Based on the error percentage, weak and strong turbulence cases perform about the same. Resultant intensity measurements are also taken from the SLM output. Theory in a weak fluctuation regime requires that the log normal distribution predict intensity probability. These distributions are achieved in strong turbulence cases where peak-to-valley intensities are higher and easily distinguishable by the CCD targetboard. Log normal intensity distributions are not as well verified in weak turbulence because of the difficulty of measuring low intensity variation by the targetboard.

4.5   Wavetrain Simulation Comparison

To aid in proper system behavior evaluation, a computer simulation using Wavetrain is run alongside the lab bench setup to observe output intensity. Each turbulence case is verified using the same physical dimensions in the simulation that are present on the lab bench. System intensity output is shown in Figures 39 through 43.

Intensity patterns are somewhat similar to real intensity patterns output from the lab bench system. The main turbulence features concerning areas of high intensity are apparent and become smaller as turbulence increases. A qualitative comparison between the
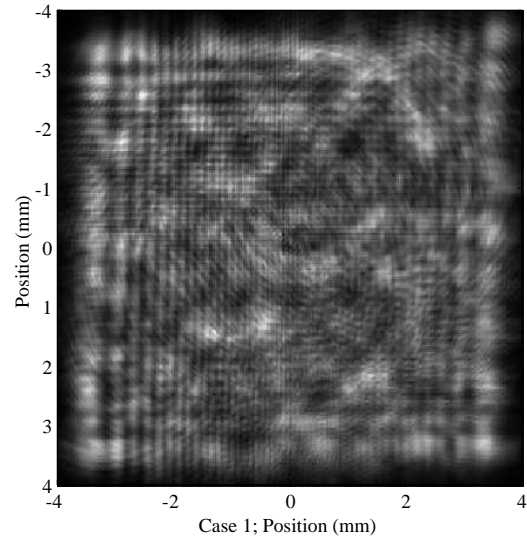
Figure 39   Simulated intensity pattern at output of aberrating system for Case1
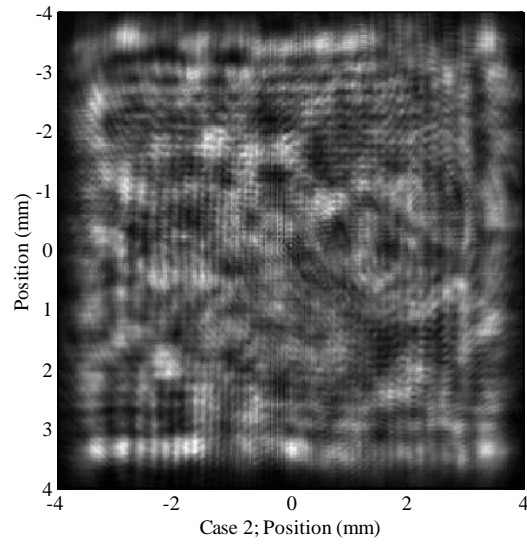
Figure 40   Simulated intensity pattern at output of aberrating system for Case 2
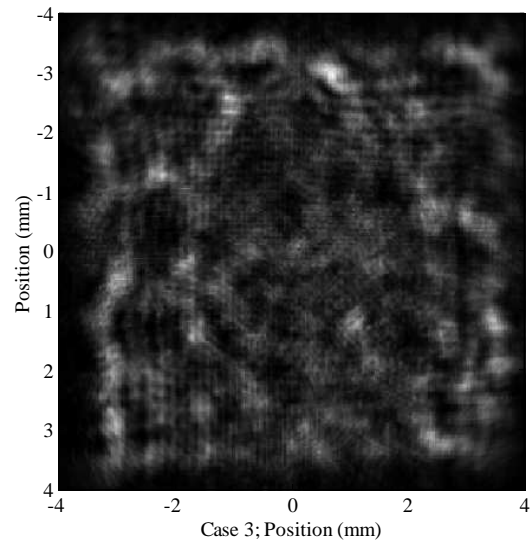
Figure 41   Simulated intensity pattern at output of aberrating system for Case 3
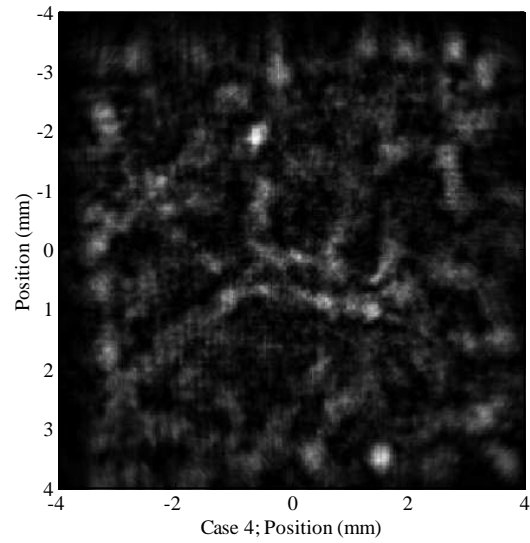
Figure 42   Simulated intensity pattern at output of aberrating system for Case 4

57
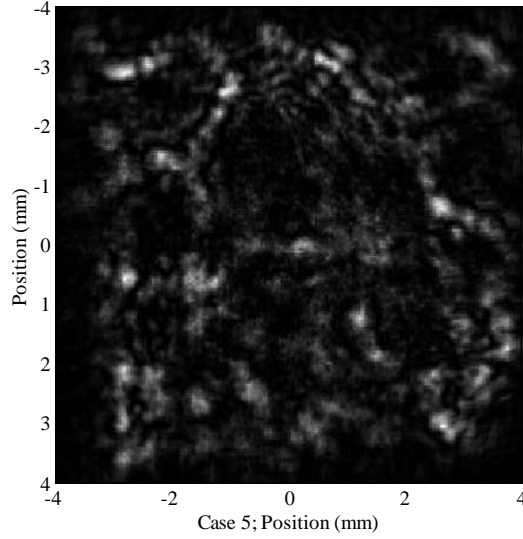
Figure 43   Simulated intensity pattern at output of aberrating system for Case 5

intensity patterns of the two systems reveals that general turbulence behavior is acceptable between the lab bench system and the computer simulation.

4.6   Summary

Data collected over five turbulence cases has been presented and evaluated using the structure function, intensity distribution, and computer simulation. Phase screens loaded to the SLM to create desired turbulence effects compare well to theory with respect to their structure function. Similarly, phase measurements of output light evaluated using the Kolmogorov structure function show that proper behavior is present, but with limited accuracy. Intensity measurements yield some uncertain results in part because of the inadequacies of the CCD targetboard. Stronger turbulence registered distributions that matched log normal theory, while weaker turbulence produces intensity variations that are more difficult to characterize. Distributions for weak turbulence remotely resembled the log normal distribution. These results and interpretations lead to several important conclusions about the quality of the atmospheric simulation system.

58

V. Conclusions

5.1 Introduction

Research efforts reported here set out to develop a device for testing and evaluating laser detection systems for a variety of turbulence conditions so that repeatable tests can be performed in the lab to reduce the need for expensive and complex field testing. Motivation for this research is due to the proliferation of laser devices for sensing, tracking, and harming aircraft. For atmospheric simulation, a spatial light modulator (SLM) is employed to manipulate laser light. The SLM uses a liquid crystal material to affect a change on the index of refraction through which laser radiation travels. A large disconnect exists between laser detection operating environments and in-door lab facilities with respect to size. Scaling an optical system down to model a larger system is discussed from the point of view of diffraction strength and turbulence scaling. Three objectives underlie this research. The first objective is to demonstrate that atmospheric effects can be introduced into an optical system using a spatial light modulator. The second objective is to characterize the behavior and response of the SLM necessary to achieve acceptable results. The third objective is to validate the system by comparing its end product to well based theory with respect to random statistics. Finally, an assessment of system quality is made based on collected data and interpretations of trends and relationships within the data. By recognizing shortcomings of system performance, recommendations are made to improve future operation.

5.2 Conclusions Based On Results

In this research, five turbulence scenarios are explored using the aberrating system. Measurements of structure and intensity distribution are completed to judge how well the system operates. Scenarios are arranged so the coherence length decreased from Case 1 to Case 5, indicating an increase in turbulence strength from Case 1 to Case 5. Judging system performance with respect to each propagation scenario is necessary because each case operates in a unique way.

Phase measurement errors are significant for all scenarios, ranging from 15.7% in Case 4 to 32.0% in Case 5. Part of this error comes from wavefront sensor measurement uncertainty, but some may also have origins in the SLM. Despite this error, the structure functions are monotonically increasing and approach the 5/3 power relationship. The system has near acceptable performance in its phase behavior. Verification yielded similar results in intensity. Comparing the lognormal distribution to the intensity distribution gave mean square error results ranging from 1.16×10^{-4} for Case 4 to 5.70×10^{-4} for Case 3. The lognormal distribution was easier to verify in stronger turbulence where the CCD targetboard was better equipped to measure large variance in intensity. Sources of error here include distorted intensity caused by interference from the targetboard cover glass. Though the amount of error in the data compared to the lognormal distribution is significant, these intensity distributions do have the form and properties of log normal curves. Intensity measurements assert a roughly satisfactory system behavior in weak to strong turbulence cases. Computer simulation verified most general system behavior in that stronger turbulence created smaller patches of high intensity over expanses of low intensity.

Two evaluations were conducted of the aberrating system, each pointing to the fact that the SLM setup is capable of representing the atmosphere's index of refraction variations, but only with limited accuracy. With regard to the scenarios tested, system performance was relatively constant across weak and strong turbulence cases. The atmospheric simulator has potential as a viable test tool, but as it stands, several qualities need to be improved upon.

5.3 Research Advances and Implications

Some system technology and concepts in this research have been used in unique ways. Their integration has lead to a functioning product that offers benefits to the Air Force. Considering the system and its component parts reveal alternate applications in which this research is beneficial.

Using the spatial light modulator to implement turbulence screens is a novel application that shows promise as a viable tool for test and evaluation. Many adaptive optics

systems strive to correct atmospheric influences. Working in the opposite direction requires choosing an atmospheric model and representing atmospheric influences in the form of phase screens. Creating phase screens requirs effective sampling of a power spectrum to induce proper behavior. Using non-uniform sampling of the model (rather than uniform) is a relatively new concept that yields improvements in fabricated phase screens.

The aberrating system demonstrated in this research has positive implications for the Air Force. Not only does the system allow testing in a convenient lab environment, it also has the potential to reduce development time and cost for laser warning systems. With the ability to select a variety of different laser scenarios and turbulence strengths, laser warning systems can be tested quickly and without the repeated cost of aircraft resources and test beds. These benefits are significant to system development in the Air Force.

Several applications are possible in the spatial light modulator that are worth mentioning. This research covered a turbulence generation application. Additionally, the SLM may be used as a wavefront correction device in monochromatic optical systems with static or slowly varying aberrations. Further, the phase manipulating ability of the SLM is flexible enough that expensive or complex optic elements could be totally replaced. The SLM is a versatile device keeping in mind its use only in very narrowband light.

5.4 Recommendations for Future Work

As the atmospheric simulator does not achieve ideal performance, several improvements to the current system are available. In addition, certain recommendations for future systems exist that will extend the range of turbulence representation and accuracy. These recommendations are all achievable using current available technology.

Several measurement limitations and errors are encountered in this research that hinder system evaluation. Difficulty is encountered in aligning the wavefront sensor so that an ideal calibration could be achieved. A simple solution to this problem is available in using more precise steering mirrors to direct the beam to the aperture of the wavefront sensor. With the current mirrors, tilt is zeroed by hand to within half of one wavelength. Eliminating this tilt allows more accurate measurement of the wavefront and better cal-

61

culation of the resulting structure function. Also, the CCD targetboard's low sensitivity prohibits accurate intensity variation measurement for low turbulence cases. The targetboard should be replaced by a power meter with a resolution of fractions of micro-watts. With this device, a small portion ($\leq 1\,\mathrm{mm}^2$) of the output intensity pattern could be isolated and measured for each turbulence screen. This would eliminate the interference issue with the targetboard cover glass and provide more accurate measurements for low turbulence cases.

Recommendations for future atmospheric simulation systems include devising a method to take phase measurements of laser propagation through real atmospheric paths. From these measurements, optical path difference maps could be created to load onto the SLM for exact duplication of turbulence cases. Another possibility is to use a feedback control system from the wavefront sensor to the SLM. Minor phase abnormalities were noticed from the SLM when calibrating the wavefront sensor. A possible source of these abnormalities is inter-pixel influence from the E-field controlling the liquid crystal orientation. A feedback system could be used to tell the SLM how to correct for its own abnormalities. Additionally, a real-time simulation could be executed with the SLM system. To enable real-time simulations, the SLM displays a sequence of scrolling turbulence screens at a specified frame rate to match wind velocity from Taylor's frozen flow hypothesis. The maximum frame rate of the SLM in this research is $75\,\mathrm{Hz}$ to $150\,\mathrm{Hz}$ depending on temperature and other factors [9]. This capability is on the order of the refresh rate needed to represent a moderately changing atmosphere at $100\,\mathrm{Hz}$. Finally, multiple SLMs could be used in an atmospheric simulator to implement phase distortion at multiple locations along the propagation path. This setup would more closely match distortion observed in the real world. Together with the conclusions of this research, the above recommendations make an atmospheric simulation tool viable for lab-based work.

Appendix A. Phase Screen Generation Code

A.1   Introduction

Controlling the atmospheric simulator consists mainly of loading proper phase screens to the spatial light modulator (SLM). Creating these screens is done through Matlab using several valuable functions and m-file scripts. These functions and scripts are presented here to facilitate future work and experiment repeatability. Three main programs are presented. "`PropScen.m`" calculates r_o for the propagation scenario in both real size and scaled SLM size. It also calculates the Rytov variance of the scenario. "`SLMTrblGen.m`" initially creates screens for the SLM with a biased tilt. "`SLMTrblReGen.m`" uses pre-generated power spectrum coefficients to create exact duplicates of previously generated screens with the option of removing the tilt bias.

A.2   PropScen.m

The following code comprises the "`PropScen.m`" function:

```
function [scenario] = PropScen(RunName,DataPath,lambda,...
    Hstart,Hend,PropDist,PropDx,HDx)
% [SCENARIO] = PROPSCEN(RUNNAME,DATAPATH,LAMBDA,...
% HSTART,HEND,PROPDIST,PROPDX,HDX)
% Coherence Distance (Ro) Calculator using H/V 5/7 model
% Author:  Matthew Brooks
% Last Updated:  1/21/04
%
% This function uses the Huffnagel-Valley 5/7 model to
% compute the path integrated Cn942 value and then
% calculates Ro.  (Ro is used as an input to the F.S.
% screen generation algorithm)
% INPUTS:
% RunName:  (string) Name of to be given to the run
% DataPath:  (string) Path where run will be located
% lambda:  wavelength of light (m)
% Hstart:  starting altitude of scenario (low) (m)
% Hend:  ending altitude of scenario (high) (m)
% PropDist:  propagation distance in scenario (m)
% PropDx:  propagation step size (m) This variable
% is only used if the starting and ending heights
% are equal.
% HDx:  height step size (m) This variable is only
```

63

```
% used when the starting and ending heights are
% different.
% OUTPUTS:
% Ro:  Coherence Length (cm)
% RoSLM: Coherence Length (cm) for SLM assuming the
% SLM has diameter .768 cm and the scenario has
% diameter 25.4 cm
% RytovVar:  Rytov variance dictating the
% weak fluctuation regime
% All inputs and outputs are save in the file [RunName].mat
% in the DataPath directory
% RunName = 'Run1'
% DataPath = 'D:\SLMData\'
% lambda = 632.8e-9;
% Hstart = 1;
% Hend = 1;
% PropDist = 1e3;
% PropDx = .25;
% HDx = .25;
%
k = 2*pi/lambda; % Wave number
theta = acos((Hend - Hstart)/PropDist); % Angle from ground
%
if Hstart == Hend
    z = 0:PropDx:PropDist;
    h = ones(1,length(z))*Hstart;
else
    h = Hstart:HDx:Hend;
    z = h/cos(theta);
end
v = 21; % Wind velocity for H-V 5/7 model
A = 1.7e-14; % Ground Cn2 for H-V 5/7 model
%
% H-V model
Cn2 = .00594.*(v/27).942.*(1e-5.*h).9410.*exp(-h/1000) + ...
    2.7e-16.*exp(-h/1500) + A.*exp(-h/100);
%
% Path integrated Cn942
Cn2Path = sum(Cn2*(z(2)-z(1)));
RHOpl = (1.46*k942*Cn2Path).94(-3/5);
%
% Coherence length (cm)
Ro = 2.1*RHOpl*100;
RoSLM = .768*Ro/25.4;
%
```

```
% Rytov Variance
if Hstart == Hend
    RytovVar = 1.23*(Cn2Path/PropDist)*k94(7/6)*PropDist94(11/6);
else
    RytovVar = 1.23*mean(Cn2)*k94(7/6)*PropDist94(11/6);
end
%
% Save the scenario data
scenario.RunName = RunName;
scenario.lambda = lambda;
scenario.Hstart = Hstart;
scenario.Hend = Hend;
scenario.PropDist = PropDist;
scenario.Ro = Ro;
scenario.RoSLM = RoSLM;
scenario.RytovVar = RytovVar;

save([DataPath RunName '\' RunName],'scenario');
```

The "PropScen.m" function saves its inputs and outputs into a Matlab file so that they can be recalled for later use.

A.3 SLMTrblGen.m

The following code comprises the "SLMTrblGen.m" script file:

```
% SLM Turbulence Screen Generator
% Author:  Matthew Brooks
% Last Upadated:  1/21/04
% This m-file creates multiple turbulence screens for
% a 512x512 SLM using the Fourier Series of a created
% power spectrum.
%
% The INPUTS are:
% ScreenAmt:  Number of screens to create
% FileChoice:  Set to 1 to create bitmaps and sif's
% SaveInfo:  Set to 1 to save the input variables to
% .mat file for later use, otherwise set to 0.
% FrozenFlow:  Choose whether to move the screen for
% each iteration.  Set to 1 to move the screens.
% XTrans:  The number of pixels (samples) to move the
% screen in the x-direction for each iteration.
% YTrans:  The number of pixels (samples) to move the
% screen in the y-direction for each iteration.
```

```
% XTilt:  Waves of tilt in the x-direction in order to steer
% the beam off of the zero order diffraction from the SLM
% YTilt:  Waves of tilt in the y-direction for same purpose
% RunName:  (string) Name to give the run.  Used to name the
% sif file, screen bitmaps, and data file, but only
% used when FileChoice is set to 1.
% DataPath:  (string) Path where Runs are located.  Used to
% save the screen bitmaps, sif file, and data file, but
% only used when FileChoice is set to 1.
% Tx:  Sample spacing for screen (m)
% Ns:  Number of samples for the screen
% T.N: Number of FS Coeff's
% T.fmin:  Min spatial frequency of spectrum (m94-1)
% T.fmax:  Max spatial frequency of spectrum (m94-1)
% T.r0:  Coherence length for screen (m), set to 'Ro' or
% 'RoSLM' if you are using the value scenario and values
% computed by "PropScen.m"
% T.lo:  Inner scale of turbulence (m)
% T.Lo:  Outer scale of turbulence (m)
% T.Model:  Spectrum turbulence model to use
%
% The screens are always saved
% in the Matlab variable "SLMScreen" in gray levels (0:255) if
% no bitmaps are created or in bitmap units (0:1) if bitmaps
% are created.
% Note:  This m-file requires the functions:  mkPSD, FSCoeff,
% FSscrnREAL, and rad2val.  The first three are curtosey of
% Eric Magee (Mission Research Corporation, August 2003)
%
ScreenAmt = 100;
FileChoice = 1;
SaveInfo = 1;
FrozenFlow = 1;
XTrans = 6;
YTrans = 6;
XTilt = -95;
YTilt = 95;
RunName = 'Run5';
DataPath = 'D:\SLMData\';
Tx = 15e-6;
Ns = 512;
T.N = 64;
T.fmin = 1/30000;
T.fmax = 1/Tx;
T.r0 = 2.6585e-3;
```

```
T.lo = 0;
T.Lo = inf;
T.Model = 'Mod';
%
% If "PropScen.m" was used to create a scenario, then use that data
if ischar(T.r0)
    load([DataPath RunName '\' RunName]);
    if T.r0 == 'RoSLM'
        T.r0 = scenario.RoSLM/100; % Convert from (cm) to (m)
        Tx = 15e-6;
        Ns = 512;
        if SaveInfo == 1; SaveInfo = 2; end
    elseif T.r0 == 'Ro'
        T.r0 = scenario.Ro/100; % Convert from (cm) to (m)
        Ns = 512
        Tx = .254/Ns;
    end
end
%
% Create screen coordinate system
x = [-Ns/2:Ns/2 - 1]*Tx; y = x;
[X Y] = meshgrid(x,y);
% Create a tilt to translate the beam off the zero order diffraction
Tilt = X.*((2*pi*XTilt)/(Tx*Ns)) + Y.*((2*pi*YTilt)/(Tx*Ns));
PSD1 = mkPSD(T); % Create the Power Spectral Density
C = FSCoeff(PSD1); % Generate coefficients for FS
%
% Store input varibles and save as a .mat file
if SaveInfo == 2;
    ScreenLength = Ns*Tx;
    save([DataPath RunName '\' RunName],'RunName','scenario','C',...
        'XTrans','YTrans','ScreenLength','ScreenAmt');
elseif SaveInfo == 1
    ScreenLength = Ns*Tx;
    save([DataPath RunName '\' RunName],'RunName','C','XTrans',...
        'YTrans','ScreenLength','ScreenAmt');
end
%
if FrozenFlow 126= 1 % Stop screen from scrolling if needed
    XTrans = 0; YTrans = 0;
end
%
if FileChoice == 1 % Create sequence file and bitmaps
    fid = fopen([DataPath RunName '\' RunName '.sif'],'w');
    for m = 1:ScreenAmt
```

```matlab
            S = FSscrnREAL(x+(Tx*XTrans*(m-1)),y+(Tx*YTrans*(m-1)),C);
            S.g = mod(S.g + Tilt,2*pi); % modulate between 0 and 2pi
            SLMScreen = rad2val(S.g,[0:255]);
            SLMScreen = SLMScreen/255;
            name = [DataPath RunName '\SLMScreen\' RunName '.'...
                num2str(m) '.bmp'];
            imwrite(SLMScreen,name,'bmp');
            fprintf(fid,'%s\n',['C:\Blink\TestRuns\' RunName '.'...
                num2str(m) '.bmp' ', C:\Blink\LUT_files\AFITSLM.LUT']);
        end
        fclose(fid);
else % Just create the screens as Matlab variables
    for m = 1:ScreenAmt
        S = FSscrnREAL(x+(Tx*XTrans*(m-1)),y+(Tx*YTrans*(m-1)),C);
        S.g = mod(S.g + Tilt,2*pi); % modulate between 0 and 2pi
        SLMScreen(:,:,m) = rad2val(S.g,[0:255]);
    end
end
%%%%%%%%%%%%%%%%%%%%% Structure Function %%%%%%%%%%%%%%%%%%%%%%%%%
frames = ScreenAmt;
SumStrct = 0;
for m = 1:2
    % Recreate a screen
    screen = SLMTrblReGen(1,RunName,DataPath,m,m,...
        [RunName 'NT.' num2str(m) '.bmp'],[DataPath RunName '\']);
    Astrfcn = DataStruct(screen,...
        [-(512/2 -1)*15e-6:15e-6:512/2*15e-6],15e-6);
    Dstrfcn = DataStruct(screen',...
        [-(512/2 -1)*15e-6:15e-6:512/2*15e-6],15e-6);
    SumStrct = SumStrct + Astrfcn.g + Dstrfcn.g;
    disp([num2str(m) ' of ' num2str(frames) ' complete.']);
end
for m = 3:frames
    % Recreate a screen
    screen = SLMTrblReGen(0,RunName,DataPath,m,m);
    Astrfcn = DataStruct(screen,...
        [-(512/2 -1)*15e-6:15e-6:512/2*15e-6],15e-6);
    Dstrfcn = DataStruct(screen',...
        [-(512/2 -1)*15e-6:15e-6:512/2*15e-6],15e-6);
    SumStrct = SumStrct + Astrfcn.g + Dstrfcn.g;
    disp([num2str(m) ' of ' num2str(frames) ' complete.']);
end
DRun5.g = SumStrct/(2*frames);
DRun5.x = Astrfcn.x;
%
```

68

```
% Calculate Kolmogorv Spectrum
load([DataPath RunName '\' RunName]);
DRun5.DK = turbconst(6.88).*(DRun5.x./C.PSD.T.r0).94(5/3);
%
% Calculate the Mean Square Error
DRun5.e = sum((DRun5.DK - DRun5.g).942)/length(DRun5.x)

save([DataPath RunName '\' RunName],'DRun5','-append')
```

Screens can be saved as Matlab variables or bitmaps, but may only be loaded to the SLM in bitmap form.

A.4 *SLMTrblReGen.m*

Below is the code for the Matlab function, "SLMTrblReGen.m."

```
function [screen] = SLMTrblReGen(FileChoice,RunName,...
    DataPath,start,stop,XTilt,YTilt,SaveName,SavePath)
% [Screen] = SLMTRBLREGEN(FILECHOICE,RUNNAME,...
% DATAPATH,START,STOP,XTILT,YTILT,SAVENAME,SAVEPATH)
% SLM Turbulence Screen Creator from Previous Data
% This function recreates turbulence screens that were used
% on a 512x512 SLM. The SLM screens had a tilt added to
% steer the beam away from the zero-order diffraction spot.
% In order to look at the screens and process them, this
% tilt is not added here so that the screens are in their
% "regular" form.  Bitmaps created from this m-file are
% not useful on the SLM because of the zero-order
% diffraction spot.
%
% The INPUTS are:
% FileChoice:  Set to 1 to create bitmaps.  Otherwise,
% the screens are stored in matlab variables
% RunName:  The name of the run to be recreated
% DataPath:  The path to the data where characteristics were
% stored.
% start:  Number of the first screen to be recreated.
% stop:  Number of the last screen to be recreated.
% XTilt:  Waves of tilt to add to the screen to steer the
% beam away from the zero order diffraction (X-dir)
% YTilt:  Waves of tilt to add to the screen to steer the
% beam away from the zero order diffraction (Y-dir)
% SaveName:  File name to give recreated screen
% SavePath:  Path to save recreated screens
```

```
% If no bitmaps are created, the output is:
% screen:  The array describing the screen (512x512)
% NOTE: This function requires "FSscrnREAL.m" to run.
% Author:  Matthew Brooks
% Last Upadated:  1/25/04
% FileChoice = 1;
% RunName = 'Run1';
% DataPath = 'D:\SLMData\';
% start = 1;
% stop = 100;
% SaveName = 'PreRun2';
% SavePath = 'D:\SLMData\Run1\SLMScreen\';
%
load([DataPath RunName '\' RunName]); % Load the data from previous runs
Ns = 512;
Tx = ScreenLength/Ns;
%
% Create screen coordinate system
x = [-Ns/2:Ns/2 - 1]*Tx; y = x;
[X Y] = meshgrid(x,y);
%
% Create a tilt to translate the beam off the zero order diffraction
Tilt = X.*((2*pi*XTilt)/(Tx*Ns)) + Y.*((2*pi*YTilt)/(Tx*Ns));
if FileChoice == 1
    for m = start:stop
        S = FSscrnREAL(x+(Tx*XTrans*(m-1)),y+(Tx*YTrans*(m-1)),C);
        S.g = mod(S.g + Tilt,2*pi); % modulate between 0 and 2pi
        SLMScreen = rad2val(S.g,[0:255]);
        SLMScreen = SLMScreen/255;
        name = [SavePath SaveName '.'  num2str(m) '.bmp'];
        imwrite(SLMScreen,name,'bmp');
    end
    screen = SLMScreen;
else
    for m = start:stop
        S = FSscrnREAL(x+(Tx*XTrans*(m-1)),y+(Tx*YTrans*(m-1)),C);
        screen(:,:,m-start+1) = S.g;
    end
end
```

Like "SLMTurblGen.m," re-created screens can be saved as Matlab variables or as bitmaps.

Appendix B.   Wavetrain System Layout

B.1   Introduction

Wavetrain is a versatile wave optics code used in this research to help validate the atmospheric simulator.   Wavetrain is a stand-alone program, but can be run in Matlab as a "mex" system using functions provided with the Wavetrain software package.   It is important to present the Wavetrain system created for use in this research to assist future work.   Wavetrain has two components that makeup a simulation: the System Editor and the Runset Editor.   In the system editor, a graphical user interface connects optical or system components through which the simulated field moves.   In the Runset Editor, values to parameters such as propagation distance and sample frequencies are setup for a particular "run" of the system.   Additionally, a Matlab script is created to more easily control the simulation and create multiple runs where the phase screen is changed for each run.   Each of these three components is explained below.

B.2   System Editor

Simulating the aberrating system in this research was started in the System Editor.   Referring back to Figure 12 in Chapter III, the collimated laser beam is represented by a plane wave source immediately followed by a circular aperture ("Source1" and "Source1Ap").   The field is then sent through a vacuum propagation element, "VPath1," and to a propagation check element, "CheckProp1," to observe the field just before contact with the spatial light modulator (SLM). The SLM itself is represented by an optical path difference element, "OPD1," and a square aperture element, "Apodizer." The optical path difference accepts the same bitmaps loaded to the SLM (except that the biased tilt is not added here), while the apodizer describes the square aperture of the SLM.   The 83% fill factor could be simulated as well but would have required describing each pixel on the SLM with at least four pixels to obtain a fill factor of only 50%.   Additional pixels are needed for larger fill factor representations.   The array size needed for a loosely accurate representation (75% fill factor) is 2048×2048 which requires too much processing time. So a 100% fill factor is assumed to keep the array size to 512×512, and there was no

71

Param. Name	Description
wavelength	Wavelength of source light (m)
SrcDiam	Diameter of Source1 (m)
PropNXY1	Number of samples across length of field propagated from Source1 to SLM
PropDXY1	Sample spacing describing field from Source1 to SLM (m)
PropDist1	Propagation distance from Source1 to SLM (m)
SLMNXY	Number of samples across length of SLM
SLMDXY	SLM pixel pitch (m)
PropNXY2	Number of samples across length of field propagated from SLM to Sensor1
PropDXY2	Sample spacing describing field from SLM to Source1 (m)
PropDist2	Propagation distance from SLM to Sensor1 (m)
SLMAp	An array that describes the transmission of the SLM aperture (in this case 0s and 1s)

Table 5   System parameters used in the Wavetrain simulation

need for a bias tilt added to each turbulence screen. From the apodizer, the field is sent through a second vacuum propagation, "VPath2." Finally, the field contacts an E-field sensor, "Sensor1," that allows both amplitude and phase to be output from the system, although this element is physically unrealizable in the real world. The System Editor passes the created system to the Runset Editor so that system parameters can be assigned default values.

B.3   Runset Editor

Because the system is ultimately controlled in a Matlab environment, the Runset editor is only briefly used to set default parameter values and several other options in the system. The parameters of the simulated system and a short description can be found in Table 5. An example of the Runset Editor window is shown in Figure 44.

Additionally in the Runset editor, the available outputs are displayed so that the user may choose which outputs are recorded for viewing. For this system, "CheckProp1" and "Sensor1" are the available outputs. Once all above parameters and options are set, the run is saved so that it can be converted to a "mex" system for use in Matlab. This process and running the simulation is covered in the next section.
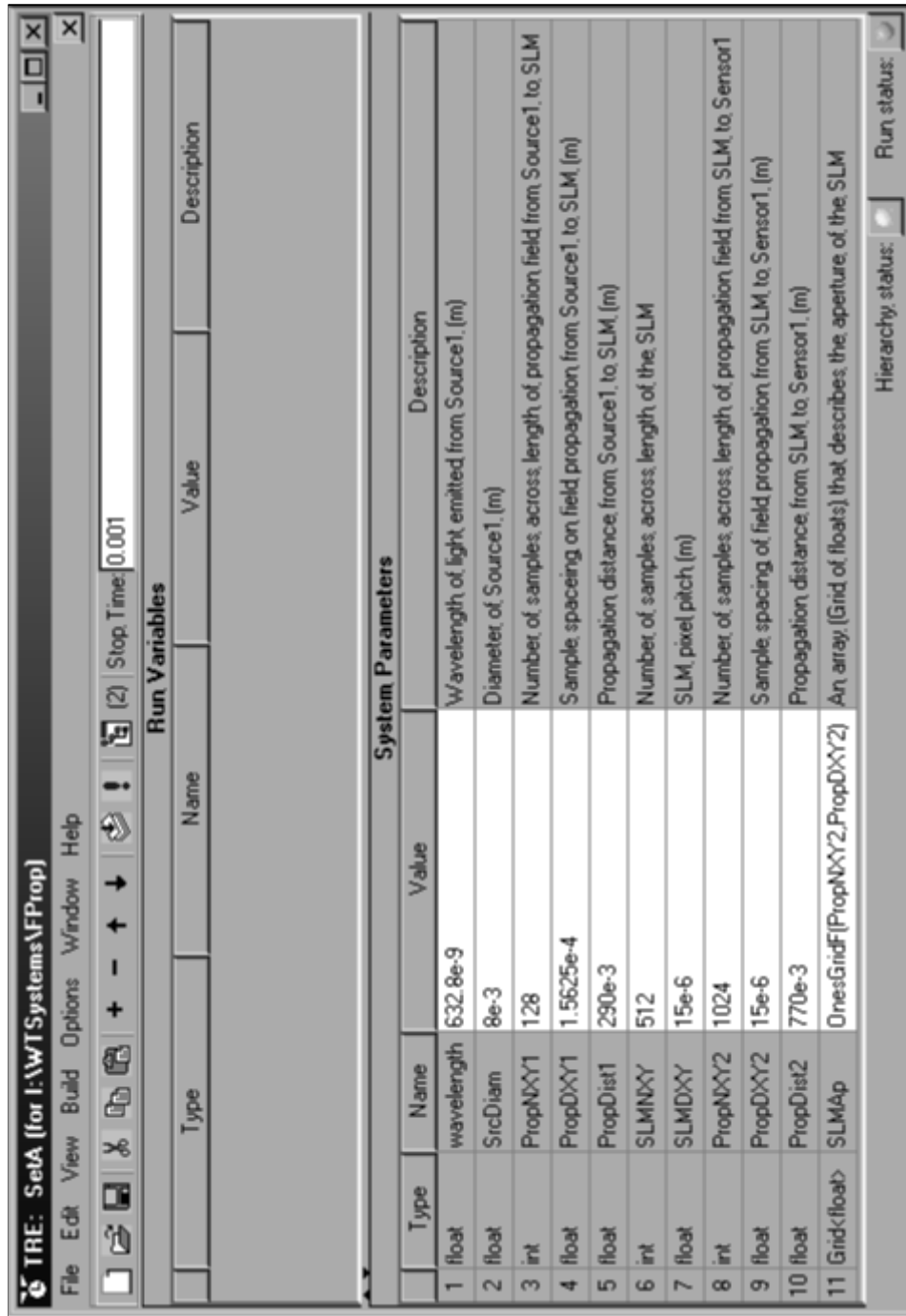
Figure 44   Wavetrain Runset Editor window with simulation parameters displayed

TRE: SetA (for I:\WTSystems\FProp)

File Edit View Build Options Window Help

Run Variables

Type	Name	Value	Description

(2) Stop Time: 0.001

System Parameters

	Type	Name	Value	Description
1	float	wavelength	632.8e-9	Wavelength of light emitted from Source1. (m)
2	float	SrcDiam	8e-3	Diameter of Source1. (m)
3	int	PropNXY1	128	Number of samples across length of propagation field from Source1. to SLM
4	float	PropDXY1	1.5625e-4	Sample spaceing on field propagation from Source1. to SLM. (m)
5	float	PropDist1	290e-3	Propagation distance from Source1. to SLM. (m)
6	int	SLMNXY	512	Number of samples across length of the SLM
7	float	SLMDXY	15e-6	SLM pixel pitch (m)
8	int	PropNXY2	1024	Number of samples across length of propagation field from SLM to Sensor1
9	float	PropDXY2	15e-6	Sample spacing of field propagation from SLM to Sensor1. (m)
10	float	PropDist2	770e-3	Propagation distance from SLM to Sensor1. (m)
11	Grid<float>	SLMAp	OnesGridF(PropNXY2,PropDXY2)	An array (Grid of floats) that describes the aperture of the SLM

Hierarchy status: Run status:

73

A simulation created in Wavetrain is converted to a "mex" system so that it can be executed entirely from Matlab's user interface. This conversion is advantageous for users already familiar with Matlab's abilities. It also allows a large variety of post-processing and graphic displays that are available in Matlab. The Wavetrain software package comes with all the Matlab scripts needed to execute and manipulate a Wavetrain simulation. The first step in this process is to run the "tmxmkdll" command on the simulation to create the Matlab "mex" system. From here, a Matlab script file is written to control and run the simulation. Any parameters, inputs, and outputs can be manipulated using this script file. The script written for the aberrating system simulation is found below. All values to the system parameters found in Table 5 are near the beginning of the script.

```
% Mex Interface file to control FProp Wavetrain Simulation
% Author:  Matthew R. Brooks
% Last Updated on 1/27/04
% Create .dll file for mex system.  Execute the command in the box below
% each time the system FProp is changed (either the
% system itself or the runset).
% NOTE: Make sure ALL file name references in this m-file match
% the file name in the box below.
%%%%%%%%%%%%%%%%%%%%%%%%%%%%
% tmxmkdll('FPropRunSetA') %
%%%%%%%%%%%%%%%%%%%%%%%%%%%%
%
% Set the System Parameters
params.wavelength = 632.8e-9; % Wavelength of light (m)
params.SrcDiam = 7.68e-3; % Diameter of source (m)
params.PropNXY1 = 512; % Number of samples for 1st propagation
TVLnProp1 = 20e-3; % Transverse length of field for 1st propagation
% Sample spacing for 1st prop.  (m)
params.PropDXY1 = TVLnProp1/params.PropNXY1;
params.PropDist1 = .29; % Prop distance b/n source and SLM (m)
params.SLMNXY = 512; % Number of pixels across SLM
params.SLMDXY = 15e-6; % Pixel pitch of SLM (m)
params.PropNXY2 = 512; % Number of samples for 2nd propagation
TVLnProp2 = 3e-3; %Transverse length of field for 2nd propagation
% Sample spacing for 2nd prop (m)
params.PropDXY2 = TVLnProp2/params.PropNXY2;
params.PropDist2 = .77; % Prop distance b/n the SLM and sensor (m)
params.SLMAp.x = (-params.PropNXY2/2+1:params.PropNXY2/2)*params.PropDXY2;
```

```
params.SLMAp.y = params.SLMAp.x;
SLMApX = params.SLMAp.x > -3.84e-3 & params.SLMAp.x < 3.855e-3;
SLMApY = (params.SLMAp.y > -3.84e-3 & params.SLMAp.y < 3.855e-3)';
params.SLMAp.g = SLMApY*SLMApX;
clear SLMAp
%
% Set the minimal stop time needed to get light at the detector
StpTime = 1.1e-3 + (params.PropDist1 + params.PropDist2)/3e8;
%
% Intitialize the system and get the grid spacing
tmxh = tmxcreate('FPropRunSetA',params);
trfname = tmxh.trfname;
%
%Create the input field
Uin.x = (-params.PropNXY1/2+1:params.PropNXY1/2)*params.PropDXY1;
Uin.y = Uin.x;
Uin.g = ones(length(Uin.x),length(Uin.y)).*exp(j*0);
%
% Create the OPD Map
DataPath = 'C:\Documents and Settings\Matthew\My Documents\SLMData\';
RunName = 'Run19';
OPD = MZAScrnRead(params.wavelength,params.SLMDXY,...
 RunName,DataPath,54);
%
% Run the system with the desired inputs
tmxh = tmxsetinp(tmxh,'Infield',Uin);
tmxh = tmxsetinp(tmxh,'InOPD',OPD);
tmxh = tmxrun(tmxh,StpTime);
%
% Get the outputs and clean up unwanted files
CheckImg = tmxload(tmxh,'CheckProp1.field');
SensImg = tmxload(tmxh,'Sensor1.fld');
SensImg.params = tmxh.compparams;
tmxh = tmxdel(tmxh);
delete(trfname);
%
figure(1)
subplot(121)
imagesc(CheckImg.x,CheckImg.y,(abs(CheckImg.g)).942);
title('Intensity Just Before SLM');
colormap(gray(256)); colorbar('horiz'); axis square;
subplot(122)
OPDw = OPD.g/params.wavelength; % Convert to waves of Optical Path Delay
imagesc(OPD.x,OPD.y,OPDw); colorbar('horiz'); axis square;
title('Optical Delay in Waves');
```

```
figure (2)
subplot(121)
imagesc(SensImg.x,SensImg.y,(abs(SensImg.g)).942);
title('Output Intensity')
colormap(gray(256)); colorbar('horiz'); axis square;
subplot(122)
imagesc(SensImg.x,SensImg.y,angle(SensImg.g))
title('Output Phase in Radians')

axis square; colorbar('horiz')
```

The script displays the field intensity just before the SLM, the optical path difference, the output intensity, and the output phase. These last two items are similar to what is captured by the targetboard and wavefront sensor of the lab bench experiment. These outputs allow a simple comparison between the simulated system and the lab bench system.

Bibliography

1. Andrews, Larry C. and Ronald L. Phillips. *Laser Beam Propagation through Random Media*. Belingham, WA: SPIE, 1998.

2. Goodman, Joseph W. *Introduction to Fourier Optics* (2nd Edition). New York, McGraw-Hill, 1996.

3. Andrews, Larry C. "An Analytical Model for the Refractive Index Power Spectrum and its Application to Optical Scintillations in the Atmosphere," *J. Mod. Opt.*, *39*:1849 – 1853 (1992).

4. Andrews, Larry C. and M. A. Al-Habash and C. Y. Hopen and R. L. Phillips. "Theory of Optical Scintillation: Gaussian-beam Wave Model," *Waves Random Media*, *11*:271 – 291 (2001).

5. Magee, Eric P. *Phase Screens for Long Time Series Wave Optics Simulations*. Technical Report, Mission Research Corporation, May 2003.

6. Mitra, Sanjit K. *Digital Signal Processing: A Computer-Based Approach* (2nd Edition). McGraw-Hill, 2001.

7. Collings, Peter J. and Jay S. Patel. *Handbook of Liquid Crystal Research*. New York: Oxford, 1997.

8. Yariv, Ammon and Pochi Yeh. *Optical Waves in Crystals*. New York: Wiley, 1984.

9. Boulder Nonlinear Systems, 450 Courtney Way, Unit 107, Layfayette, CO 80026. *User Manual: 512x512 SLM System* (2nd Edition), June 2003.

10. Praus, II., Bob W. *WaveTrain User's Guide Online Documentation*. MZA Associates Corporation, 2021 Gerard SE, Suite 150, Albuquerque, NM 87106, Feb 2001.

11. Hobbs, Phillip C. D. *Building Electro-Optical Systems: Making It All Work*. Wiley-Int, 2000.

12. Hecht, Jeff. *The Laser Guidebook* (2nd Edition). McGraw-Hill, 1992.

Vita

Second Lieutenant Matthew R. Brooks was born in 1979 in Newport News, Virginia. He graduated from Hampton Roads Academy in 1998. Brooks then matriculated as a "rat" at the Virginia Military Institute in Lexington, Virginia. Graduating with highest honors in 2002 and receiving his B.S. in Electrical Engineering, he accepted a commission to the United States Air Force. In August 2002, Lieutenant Brooks went active duty and was assigned to the Air Force Institute of Technology, Wright-Patterson Air Force Base, Ohio to pursue a Master of Science degree in Electrical Engineering. Upon graduation, Lieutenant Brooks will stay on at Wright-Patterson Air Force Base and work for the Air Force Research Lab, Sensors Directorate.

REPORT DOCUMENTATION PAGE

1. REPORT DATE (DD-MM-YYYY)	2. REPORT TYPE	3. DATES COVERED (From – To)
23-03-2004	**Master's Thesis**	Jun 2003 - March 2004

4. TITLE AND SUBTITLE	5a. CONTRACT NUMBER
ATMOSPHERIC SIMULATION USING A LIQUID CRYSTAL WAVEFRONT CONTROLLING DEVICE	5b. GRANT NUMBER
	5c. PROGRAM ELEMENT NUMBER

6. AUTHOR(S)	5d. PROJECT NUMBER
Brooks, Matthew R., 2nd Lieutenant, USAF	5e. TASK NUMBER
	5f. WORK UNIT NUMBER

7. PERFORMING ORGANIZATION NAMES(S) AND ADDRESS(S)	8. PERFORMING ORGANIZATION REPORT NUMBER
Air Force Institute of Technology Graduate School of Engineering and Management (AFIT/ENG) 2950 Hobson Way, Building 640 WPAFB OH 45433-7765	AFIT/GE/ENG/04-01

9. SPONSORING/MONITORING AGENCY NAME(S) AND ADDRESS(ES)	10. SPONSOR/MONITOR'S ACRONYM(S)
AFRL/SNJT Attn: Dr. Jack Parker 3050 C. Street, Hangar 4B WPAFB OH 45433 Comm: 355-9272 x1777	11. SPONSOR/MONITOR'S REPORT NUMBER(S)

12. DISTRIBUTION/AVAILABILITY STATEMENT
APPROVED FOR PUBLIC RELEASE; DISTRIBUTION UNLIMITED.

13. SUPPLEMENTARY NOTES

14. ABSTRACT

Test and evaluation of laser warning devices is important due to the increased use of laser devices in aerial applications. In this thesis, an atmospheric aberrating system is developed to enable in-lab testing of laser warning devices. This system employs laser light at 632.8nm from a Helium-Neon source and a spatial light modulator (SLM) to cause phase changes using a birefringent liquid crystal material.

Before the system can be used, the SLM phase response must be quantified to ensure proper manipulation of index of refraction. Additionally, diffraction from the SLM and real-world system scaling are addressed. Once completed, the atmospheric simulator is demonstrated and verified.

Control of the SLM is achieved by loading 256 level bitmaps which dictate the desired index of refraction changes (called phase screens). Phase screens are created using a Fourier series technique applied to an atmospheric model in the form of a power spectrum. Five laser propagation scenarios are created, each with a set of screens describing turbulence for a particular case. Outgoing radiation from the SLM is then measured using a CCD targetboard for intensity and a Shack-Hartmann wavefront sensor for phase. Comparing system output phase statistics to atmospheric theory reveals a moderate correlation in all turbulence cases indicating desired performance. Intensity statistics are compared to the log normal distribution governed by the weak fluctuation regime. An error analysis reveals that strong turbulence data matches theory but that weak turbulence data is inconclusive due to measurement precision issues. As an additional check on performance, a wave optics computer simulation is created analogous to the lab-bench design. Phase and intensity data affirm lab-bench results so that the aberrating SLM system can be operated confidently.

15. SUBJECT TERMS
Atmospheric Refraction Index, Atmospheric Turbulence, Turbulence, Aberration, Laser Applications, Wave Propagation, Infrared Early Warning Systems, Simulation

16. SECURITY CLASSIFICATION OF:			17. LIMITATION OF ABSTRACT	18. NUMBER OF PAGES	19a. NAME OF RESPONSIBLE PERSON
REPORT U	**ABSTRACT** U	**c. THIS PAGE** U	UU	92	Matthew E. Goda, Maj, USAF (ENG) **19b. TELEPHONE NUMBER** (Include area code) (937) 785-2024; e-mail: mgoda@afit.edu